

THE PENNSYLVANIA STATE UNIVERSITY
SCHREYER HONORS COLLEGE

DEPARTMENT OF BIOMEDICAL ENGINEERING

INVESTIGATION OF POLYMER MICRONEEDLES IN THE DELIVERY OF PROTEIN
DRUGS

DAVID KAUFFMAN
SPRING 2018

A thesis
submitted in partial fulfillment
of the requirements
for a baccalaureate degree
in Biomedical Engineering
with honors in Biomedical Engineering

Reviewed and approved* by the following:

Yong Wang
Professor of Biomedical Engineering
Thesis Supervisor

Jian Yang
Professor of Biomedical Engineering
Honors Adviser

Pak Kin Wong
Professor of Biomedical Engineering
Faculty Reader

* Signatures are on file in the Schreyer Honors College.

ABSTRACT

Proteins are essential biomolecules that determine various biological functions in the body. Therefore, proteins may be used as therapeutic agents in the treatment of various human diseases. However, similar to many traditional drugs, without an appropriate delivery method, it would be challenging to achieve a high therapeutic effect with minimal side effects. Drug delivery methods often suffer from problems ranging from pain and patient noncompliance to reduced drug bioactivity. Microneedle patches represent a method to combine the efficacy of hypodermic needle drug delivery and the ease of oral delivery. However, current microneedle strategies cannot fulfill the requirement of sustained drug release. Thus, the long-term goal of this project is to develop aptamer-functionalized polymer microneedle patches for protein delivery. Vascular endothelial growth factor (VEGF) was used as a model to illustrate the functionality of the polymer microneedles. A series of *in-vitro* assessments were performed to determine the mechanical strength, insertion ability, encapsulation efficiency, and bioactivity of the VEGF contained within the microneedles. *In-vivo* assessments of VEGF-loaded microneedles were performed using live mice. VEGF microneedles were successfully manufactured and resulted in the delivery of a therapeutic dose of VEGF *in-vitro*. Continuing research efforts aim to successfully deliver VEGF *in-vivo*. Additional on-going studies are focused on the improvement of the delivery modality of VEGF to enable sustained release over a defined period of time using aptamer technology. The ability to deliver bioactive proteins through the skin may provide revolutionary new treatments for a range of different pathologies.

TABLE OF CONTENTS

LIST OF FIGURES	iv
LIST OF TABLES	vi
ACKNOWLEDGEMENTS	vii
Chapter 1 Introduction	1
1.1 Literature Review	1
1.1.1 Therapeutic Protein Delivery	1
1.1.2 Aptamer-Mediated Drug Delivery	2
1.1.3 Microneedle-Mediated Drug Delivery	4
1.1.4 Microneedle Patch Design Criteria	6
1.1.5 Procedure of Microneedle Fabrication	8
1.1.6 Present Challenges of Dissolving Microneedles	9
1.2 Objective and Specific Aims	10
Chapter 2 Materials and Methods	12
2.1 Fabrication of PVP/PVA Microneedles	12
2.1.1 Creation of PDMS Molds	12
2.1.2 Preparation of Dissolving Microneedle Matrix Polymer	13
2.1.3 Casting Matrix Polymer in Microneedle Molds	15
2.1.4 Model Protein Encapsulation in Microneedle	16
2.1.5 Model Protein Fluorescence Labelling	16
2.1.6 VEGF Protein Encapsulation in Microneedle	17
2.2 Mechanical Performance Evaluation	17
2.3 Protein Drug Tertiary Structure Evaluation	17
2.4 Model Drug Release Efficiency Evaluation	18
2.5 In-Vitro Insertion Testing	18
2.6 Enzyme-linked Immunosorbent Assay (ELISA)	19
2.7 In-Vitro Endothelial Cell Tube Formation Assay	20
2.8 In-Vitro Endothelial Cell Proliferation Assay	21
2.9 In-Vitro Integrated Cell Proliferation Assay	21
2.10 In-Vivo Assay	22
2.11 Statistical Analysis	24
Chapter 3 Results and Discussion	25
3.1 Summary of Results	25
3.2 Microneedle Fabrication	25
3.3 Microneedle Mechanical Performance	27
3.4 Protein Tertiary Structure Assessment	30
3.5 In-Vitro Insertion Assessment	32
3.6 Protein Release Efficiency	34

3.7 In-Vitro Protein Bioactivity Assessment.....	35
3.8 In-Vivo Protein Bioactivity Assessment	42
Chapter 4 Conclusions and Future Research	46
4.1 Conclusions.....	46
4.2 Future Research.....	46
BIBLIOGRAPHY.....	47

LIST OF FIGURES

Figure 1. Anti-VEGF Aptamer [5].....	3
Figure 2. Microneedle Design Scheme [9]	5
Figure 3. Mechanisms of Drug Transport and Elimination [12].....	7
Figure 4. Microneedle Fabrication Scheme	9
Figure 5. Microneedle Mold	12
Figure 6. PDMS Mold containing 3:1 PVA/PVP polymer solution.	15
Figure 7. Microneedle Applicator Device.....	19
Figure 8. Schematic of MN Insertion Sites.....	23
Figure 9. SEM image of Microneedle Array. Scale bar: 1mm. Insert scale bar: 100µm.	26
Figure 10. Representative Microneedle Arrays.	26
Figure 11. Representative Microneedle Array. Scale bar: 1mm	27
Figure 12. Fracture Force per Needle of Various MN Polymer Combinations. Each result is the mean of 3 samples. The error bars represent ± 1 standard deviation from the reported mean. No statistically significant differences were observed.	28
Figure 13. Representative Force vs Extension Plot. 3:1 PVA/PVP Microneedles used for evaluation. The sharp depression observed at 27N is taken to be the fracture point.	29
Figure 14. Mechanical Strength of Protein Encapsulated Microneedles. Each result is the mean of 3 samples. The error bars represent ± 1 standard deviation from the reported mean. No statistically significant differences were observed.	29
Figure 15. BSA Fluorescence Intensity Assay. Excitation wavelength was 280 nm; emission measured from 300 to 400 nm. Denatured BSA reflects a different emission pattern compared to stock BSA and microneedle sample BSA.	31
Figure 16. BSA Fluorescence Intensity with/without PVA/PVP. The emission pattern appears similar, however the intensity magnitude of the curve associated with BSA mixed with polymer is depressed.	32
Figure 17. Fluorescently Tagged BSA Isolated to Tip-Region within Microneedle Array. Scale bar: 200 µm.	33
Figure 18. Cross-section of Mouse Skin showing maximum insertion depth. Scale bar: 200 µm.	34
Figure 19. Representative Tube Formation Positive Control. 10 ng/mL stock VEGF solution added to HUVECs. Closed loop tube formation was observed.	36

- Figure 20. Representative Tube Formation Negative Control. No VEGF was added and limited tube formation was observed.37
- Figure 21. Representative Tube Formation 10 ng/mL VEGF Microneedle. Microneedles containing 10 ng/mL VEGF were dissolved and added to HUVECs. Moderate tube formation was observed.37
- Figure 22. Representative Tube Formation 20 ng/mL VEGF Microneedle. Microneedles containing 20 ng/mL VEGF were dissolved and added to HUVECs. Cell proliferation and limited tube formation were observed.....38
- Figure 23. Representative Tube Formation 40 ng/mL VEGF Microneedle. Microneedles containing 40 ng/mL VEGF were dissolved and added to HUVECs. Cell proliferation and limited tube formation were observed.....39
- Figure 24. Cell Proliferation Assay. Each result is the mean of 3 samples. The error bars represent ± 1 standard deviation from the reported mean. A single asterisk indicates statistical significance between experimental conditions ($p < 0.05$).40
- Figure 25. Integrated Cell Proliferation Assay. Each result is the mean of at least 6 samples. The error bars represent ± 1 standard deviation from the reported mean. A single asterisk indicates statistical significance between experimental conditions ($p < 0.05$).41
- Figure 26. Insertion of Microneedles into Live Mice. A shows the shaved back of a female mouse with and without microneedle arrays inserted. B shows each of the three microneedle arrays before and after insertion into mouse skin. The scale bar shown is 200 μm43
- Figure 27. Inflammation on Dorsal Region of Mice. Day 1 was microneedle insertion. A perceptible but insignificant increase in inflammation is visible between Day 5 and Day 6. Day 3 was not captured due to technical error.44

LIST OF TABLES

Table 1. Formulations of PVP/PVA (50% by mass).....	13
Table 2. Formulations of PVP/PVA (20% by mass).....	14
Table 3. ELISA Detected VEGF Release Efficiency.....	34

ACKNOWLEDGEMENTS

I thank Dr. Yong Wang, my thesis advisor and research mentor for providing research support and guidance. I learned a plethora of skills in the three years of working in his lab that will serve me well in my future career. I also am grateful for the mentorship provided by James Coyne and other members of Dr. Wang's lab over the time that I have worked in the lab. Their advice, support, and patience during this project and other projects have enabled their success. I also thank Dr. Jian Yang and Dr. Pak Kin Wong for their service on my thesis committee.

I thank the Office of Undergraduate Education and the College of Engineering for providing summer research funding that enabled significant progress to be made on this project during the summer months. I also thank Dr. Yang and Ethan Gerhard for permission and assistance in using their mechanical testing instrument.

Finally, I am thankful to my family for their constant encouragement and support throughout my education thus far. I would not have reached this point in my education without their support.

Chapter 1

Introduction

1.1 Literature Review

1.1.1 Therapeutic Protein Delivery

Small biomolecules in the form of proteins make up a large class of drugs that have great potential to advance the current state of disease treatment. Proteins can be delivered for therapeutic or diagnostic purposes directly into the skin owing to the populations of immune cells and vasculature present [1]. One example of a diagnostic purpose of protein delivery is the delivery of protein antigens to the skin for diagnostic food allergy tests [1]. Other reported examples of protein delivery include vaccinations, signaling peptides, and growth factors [2].

A variety of proteins currently serve important roles as drugs. Proteins such as insulin, bone-morphogenic protein 2, and vascular endothelial growth factor (VEGF) serve important roles in the treatment of human diseases. One limitation of proteins as drugs is their high functional dependence on the surrounding environment and thus low overall bioactivity [3]. Temperature and pH are key factors that determine a protein's tertiary structure, therefore variation from normal physiological conditions may irreversibly alter a protein's therapeutic potential. This eliminates the possibility of oral administration. One way to bypass the gastrointestinal tract is through transdermal peptide delivery, although this method is not without challenges such as proteases, fast metabolism, opsonization, and denaturation [3]. Therefore, drug delivery systems must be developed to enable successful protein delivery to target tissues.

Vaccination represents one of the most effective means to stop the proliferation of deadly disease known to humans and involves the delivery of inactivated protein components designed to stimulate the patient's immune system to generate antibodies against the pathogen. Signaling peptides, including hormones and cytokines are also delivered to human patients for purposes of therapy and cosmetics. Common examples of hormone delivery include insulin and parathyroid hormone, but other hormones may be delivered to alter growth and development, homeostasis, metabolism, reproduction, and response to stimuli. Growth factors represent a class of molecules designed to promote proliferation, healing, and cellular differentiation.

All proteins must be delivered only in therapeutic quantities in order to be maximally effective for patients. From a hierarchical perspective, drug delivery can be accomplished through bolus or local administration to the target tissue. Bolus delivery may be useful in situations where a large quantity of drug is required in a short period of time or it is expected that a large proportion of drug will be enzymatically broken down before it reaches the target destination. Local delivery technology provides a steady flux of drug over a constrained period of time to achieve a lasting therapeutic effect. A variety of polymeric systems have been studied for local delivery of proteins. Most of them require in vivo internal implantation. The ability of delivering proteins from the surface of the body will avoid invasive internal implantation and increase patient compliance. Thus, great effort has been made in developing technologies for the microneedle-mediated drug delivery through the skin.

1.1.2 Aptamer-Mediated Drug Delivery

Nucleic acid aptamers are key molecules of interest in this study due to their ability to enable long-term sustained release of biomolecules into target tissues. At its core, nucleic acid aptamers are single-stranded oligonucleotides that are selected from oligonucleotide libraries to have high affinity and specificity against a target molecule, not unlike antibodies [4]–[7]. Traditionally, DNA aptamers are

screened from DNA libraries through systematic evolution of ligands by exponential enrichment (SELEX) [7]. These molecules exhibit tremendous potential in the field of clinical diagnosis and drug delivery owing to their high affinity, high specificity, small size, small immunogenicity, high stability, and simplicity of synthesis [7]. Antibodies have been used extensively in the past as biomolecular markers, but are limited by sensitivity to the chemical environment as well as potential immunogenic responses [5], [7]. Aptamer ligands are a relatively new class of ligands with the potential to modulate sustained drug release.

Previous work has been performed regarding microneedle delivery of aptamers for therapeutic benefit. In a study co-authored by this author, polymer microneedles were encapsulated with anti-VEGF aptamer (as shown in Figure 1) with the goal of sequestering VEGF within a tissue phantom [5]. Due to having experience with the anti-VEGF aptamer, it is used as a model system to demonstrate the development of an aptamer-functionalized microneedle patch for the sustained delivery of proteins. This has not been previously reported in the literature. In future translational studies, the aptamer-functionalized microneedle patch will be used to deliver therapeutic proteins (e.g. insulin) through the skin for biomedical applications such as the treatment of diabetes and the delivery of vaccines.

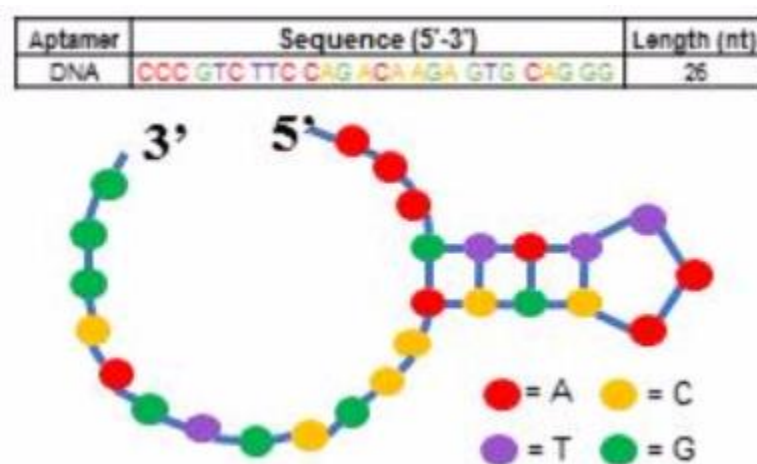


Figure 1. Anti-VEGF Aptamer [5]

1.1.3 Microneedle-Mediated Drug Delivery

To this day, the majority of drugs are delivered orally, intravenously, or intradermally through injection [2]. Oral delivery enables patients to easily administer medication to themselves with little to no assistance and is relatively pain-free. A significant caveat to oral drug delivery is the fact that orally administered drugs must be able to survive the acidic conditions of the human gastrointestinal tract and the enzymes of the intestines and liver; for many drugs, oral delivery is not feasible for this reason [2]. Injections, whether intravenously or intradermally, typically require a trained third party to administer and often are the source of patient phobias and pain [2]. Acknowledging the shortcomings of both popular drug administration routes, microneedle array patches were conceptualized to create another viable path for drug delivery. By incorporating the relative ease-of-use associated with oral administration and the efficacy associated with direct injection, microneedle patches enable for pain-free delivery of therapeutics through the stratum corneum skin layer [2]. This method of transdermal drug delivery is advantageous for the delivery of immune modulators or for the delivery of peptide growth factors. As an example of the recently published successes of microneedle patches, a recent phase 1 trial of influenza vaccine microneedle patches showed promising results and will proceed to further clinical trials [8].

Research centering on microneedle arrays in use for drug delivery and vaccination were published in 1998 and 2002, respectively. In total, roughly 800 journal articles have been published on the topic, 500 of which were published since 2010 [2]. All-in-all, microneedles have been utilized to deliver a range of small drugs including therapeutics and vaccines [9]. The literature has reported microneedles to be manufactured based on four main hierarchical design schemes: solid microneedles, coated microneedles, dissolving microneedles, and hollow microneedles as illustrated in Figure 2 [9].

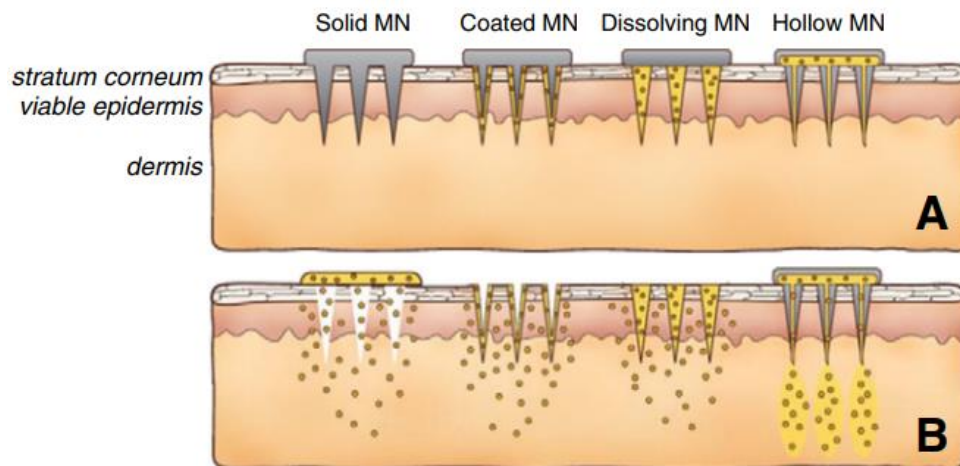


Figure 2. Microneedle Design Scheme [9]

Solid microneedles are often used to produce micro-scale perforations in the stratum corneum layer as a “pre-treatment” before a topical drug solution is applied to the skin. In this way, diffusion across the typically impermeable stratum corneum is enhanced, leading to enhanced mass transport to the body [9]. Coated microneedles are essentially identical to solid microneedles with the modification that they contain a drug formulation surrounding the needles that will subsequently dissolve away with contact with the aqueous interstitial fluid [9]. Hollow microneedles fall into the same class as solid microneedles in the sense that the microneedles themselves must be removed from the application site following treatment. Hollow microneedles enable for the delivery of aqueous drug solutions into the skin [9]. The final class of microneedles under investigation are known as dissolving microneedles, which, as the classification implies, function by dissolving entirely within the skin and releasing the encapsulated payload [9]. The major advantage of dissolving microneedles is the lack of sharps waste remaining after needle dissolution [9].

Previously reported use of microneedles includes a range of small drugs, including biotherapeutics and vaccines. Human trials have taken place using microneedle technology in the delivery of protein drugs and vaccines. Among the most proliferative uses to date is the use of hollow microneedle

technology in influenza vaccine administration [10]. Several solid microneedle solutions are currently marketed with cosmetic intentions. Active biological molecules have been delivered to the eye as well as into cells [9], [11].

1.1.4 Microneedle Patch Design Criteria

The primary design goals of microneedle patches center around enabling successful drug delivery across the primary skin barrier – the stratum corneum. A number of design objectives have been identified in the literature to create next-generation drug delivery devices that build upon successes and shortcomings of previous solutions.

The main goal in designing any drug delivery device is to enact successful and reliable drug delivery to the tissue of interest. In the design of microneedle patches, the drug must be able to be delivered across the principle barrier, the stratum corneum, which has a thickness ranging from 10 to 20 μm depending on the region of interest [2]. Additionally, the microneedle array must be capable of delivering a therapeutic dose that is consistent among manufactured lots of microneedle arrays [2].

In the design of any system designed for controlled drug release, the major goal is to provide a therapeutic level of drug for the appropriate period of time while reducing the associated toxicity of delivery [12]. Three critical factors ultimately control the drug distribution and subsequent function in the body: diffusion, convection, and elimination [12]. The mechanisms of transport and elimination specific to the skin and independent of microneedle delivery (assumption of general transdermal delivery) are further elucidated in Figure 3 [12]. Arrow a indicates possible paths of diffusion to the extra-cellular space through the stratum corneum while arrow b considers sequestration of therapeutic agent by protein binding. Arrow c considers diffusion or convective transport while arrow d considers cellular metabolism. Arrow f considers possible systemic transport or elimination.

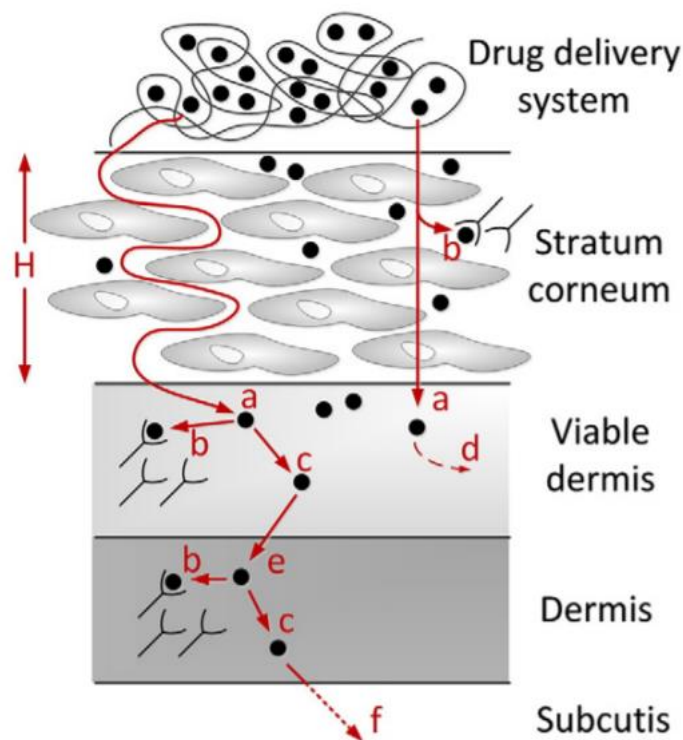


Figure 3. Mechanisms of Drug Transport and Elimination [12]

In the application of microneedles, several modifications to this model must be taken into account. The first is that the diffusion distance to the viable dermis would be greatly reduced considering the microneedle array penetrates through the stratum corneum. Because the stratum corneum is typically regarded as the rate-limiting barrier to drug transport, it is expected that microneedles are able to significantly enhance drug uptake and efficacy [13].

Secondary goals of microneedle patch design include speed of systemic drug delivery, and public health concerns such as increased access to the drug, cost savings, reduced reliance on critical infrastructure often lacking in developing nations, increased safety, and increased patient compliance [2]. It is thought that the speed of systemic drug delivery is enhanced through the use of microneedle delivery systems due to the highly vascularized nature of the skin including lymphatic drainage [2]. Microneedle arrays as drug delivery vehicles can also be designed to meet increasingly important public health

concerns such as cost, safety, availability, and patient compliance. With microneedles designed to be pressed onto the skin, less reliance on specially trained individuals is required, resulting in cost savings and increased access to the drug [2]. Dissolving microneedle designs are also capable of reducing costs associated with the disposal of sharps waste standard in the typical use of hypodermic needles.

Additional considerations include measures that increase patient compliance; this is of particular interest in the global discussion of vaccine non-compliance and the corresponding public health concerns. Microneedle arrays are designed to enact drug delivery through the skin without producing noticeable pain and to provide secondary feedback to the user to enable confirmation of drug delivery [2]. Because the needles are on the micro-scale, patient phobias of needles characteristic of traditional hypodermic needles no longer pose a concern.

With further study and experimentation, it is expected that successful production of microneedles in compliance with these design goals will enable more effective delivery of therapeutics that has the additional effect of improving public health globally.

1.1.5 Procedure of Microneedle Fabrication

Microneedle patches reported in the literature have varying designs and manufacturing processes but generally adhere to common themes. Microneedle patches can be manufactured using a variety of materials deemed to be compatible with the human body. For instance, microneedles made of metal, silicon, and polymer blends have been previously reported [2]. In nearly all cases, it is preferable to isolate the therapeutic molecule for delivery in the tip region to ensure that the complete quantity is successfully delivered through the skin.

The schematic shown in Figure 4 details the general manufacturing process for obtaining functional dissolving microneedles that was modified from previously reported literature procedures [14]. Beginning with a male master structure, secondary molds made of a common elastomer are typically

produced and later used as the template for polymer microneedle fabrication. A polymer solution containing the drug of interest is then cast onto the mold. Typically, a desiccation process and/or centrifugation process is employed to remove air pockets and ensure the needle cavities are completely full of polymer solution. The base of the microneedle array may be added stepwise or with the addition of initial polymer depending on the partition between drug and base substrate polymer desired. After an appropriate drying time, the functional microneedle array is removed from the mold.

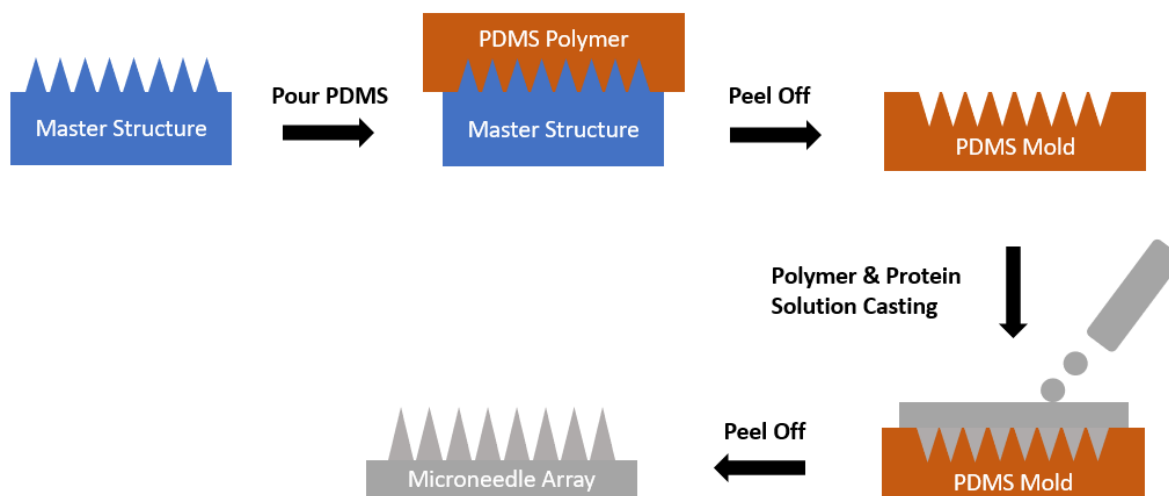


Figure 4. Microneedle Fabrication Scheme

1.1.6 Present Challenges of Dissolving Microneedles

Selection of biomaterials for use, harsh processing conditions, hard to control kinetics/rate of release, and poor mechanical strength are often cited as challenges associated with microneedle fabrication and function [15].

Biomaterials for use in transdermal drug delivery are challenging to select and each require consideration of a number of factors prior to implementation. The first barrier is the immunological host response to a foreign object being implanted inside of the body [16]. This factor is commonly assessed in

clinical trials as pain, tenderness, erythema, and swelling on a scale of 0 to 4 [17]. The next factor of consideration is the physical geometry of the biomaterial, including the shape, size, and composition [16]. The final and arguably most important factor is the biocompatibility/biodegradability of the polymer and whether it will degrade into toxic components that are unable to be cleared by the kidneys.

Dissolving microneedles are typically made of an aqueous, hydrophilic polymer solution in order to enable seamless dissolution into a generally hydrophilic, aqueous interstitial environment. As a result, the drug formulation encapsulated within these microneedles is released immediately instead of gradually over a period of time. The development of novel drug delivery systems that can encapsulate the target drug of interest and control release are the subject of ongoing investigation.

In producing microneedle arrays capable of penetrating the skin, a polymer combination with the appropriate mechanical strength must be used. Unfortunately, the strongest polymers are often incompatible with the therapeutics intended to be delivered. Therefore, many times a balance must be met between the strength of the microneedle array and the level of bioactivity of the encapsulated and later delivered therapeutic agent.

1.2 Objective and Specific Aims

The long-term goal of this study is to develop a novel aptamer-functionalized microneedle patch for local, sustained delivery of therapeutic proteins or vaccines on the skin surface. To achieve this goal, vascular endothelial growth factor (VEGF) was used as a model system to demonstrate the feasibility of the first key step in this work, i.e., the fabrication of VEGF-loaded microneedle patch, as VEGF is a well-studied protein. Specifically, polymer microneedles capable of delivering VEGF *in-vitro* and *in-vivo* will be fabricated, characterized, and evaluated. Mechanical strength, skin penetration depth, protein stability, protein encapsulation efficiency, and an assessment of

bioactivity will support the successful development of polymeric microneedle drug delivery systems capable of delivering a protein payload.

This study was accomplished through four specific aims. Specific Aim 1 entailed the fabrication of microneedles from PDMS molds using PVP/PVA. The specific concentration and volume of polymer will be optimized along with the overall manufacturing process to produce fully-formed, ideal needles with zero discontinuities. Specific Aim 2 entailed the integration of biologically active vascular endothelial growth factor (VEGF) within PVP/PVA microneedles. VEGF will be bolus released upon microneedle dissolution within the aqueous interstitial environment. Specific Aim 3 entailed the evaluation of performance in-vitro via axial load compression testing, animal skin insertion/penetration testing, enzyme linked immunosorbent assay (ELISA), endothelial cell tube formation assay, and endothelial cell proliferation assay. Mechanical testing will be conducted to ensure the microneedles have the necessary strength to penetrate human skin. Insertion testing will be employed to determine depth of penetration. ELISA will be performed to determine the bolus release efficiency of VEGF from the microneedles into solution. The endothelial cell tube formation assay and endothelial cell proliferation assay will allow for bioactivity determination of VEGF post-encapsulation in microneedles. Specific Aim 4 entailed the evaluation of performance in-vivo using animal models. Bioactivity of delivered VEGF will be confirmed by the examination of animal model skin samples post-injection.

Chapter 2

Materials and Methods

2.1 Fabrication of PVP/PVA Microneedles

2.1.1 Creation of PDMS Molds

Female microneedle molds made of polydimethylsiloxane (PDMS, Sylgard 184, Dow Corning, Midland, MI) were fabricated from male polycarbonate master structures purchased from a medical device company (Micropoint Technologies, Singapore) using a procedure adapted from the literature [18]. 4.5 grams of silicon elastomer base (4.5 grams) and 0.5 grams of silicon elastomer curing agent were added to a 15-mL tube and centrifuged for 2 minutes at 3200 rpm. The resultant mixture was poured onto a male polycarbonate master structure, vacuumed for 30 minutes, and incubated for 24 hours at 37°C. The mold was then frozen for 10 minutes at -80°C after which the mold was carefully cut out and excess PDMS was discarded. The resultant 10x10 microneedle array contained needles of 600 μm in height and 200 μm in width. One of the molds used in this study is depicted in Figure 5.

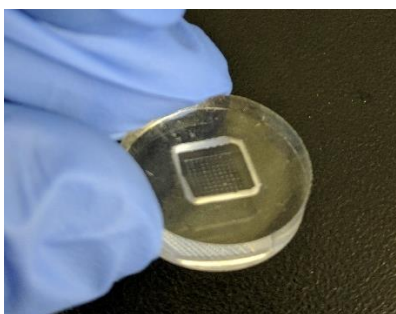


Figure 5. Microneedle Mold

2.1.2 Preparation of Dissolving Microneedle Matrix Polymer

This study utilized polyvinylpyrrolidone (PVP, 10 kDa, Sigma-Aldrich, St. Louis, MI) and polyvinyl alcohol (PVA, 9-10 kDa, Sigma-Aldrich, St. Louis, MI) as principle polymers in the preparation of the microneedle matrix solution. Over the course of this study, several combinations of PVA and PVP were prepared for further evaluation. 50% and 20% polymer solutions by mass were created over the course of experimentation. A summary of the preparations of PVA and PVP is presented in Tables 1 and 2.

Table 1. Formulations of PVP/PVA (50% by mass)

Solution	Mass of PVA	Mass of PVP	Volume of H₂O
0:1 PVA/PVP	0 g	4 g	4 mL
1:1 PVA/PVP	2 g	2 g	4 mL
1:2 PVA/PVP	1 g	2 g	3 mL
2:1 PVA/PVP	2 g	1 g	3 mL
1:3 PVA/PVP	1 g	3 g	4 mL
3:1 PVA/PVP	3 g	1 g	4 mL
1:0 PVA/PVP	4 g	0 g	4 mL

Table 2. Formulations of PVP/PVA (20% by mass)

Solution	Mass of PVA	Mass of PVP	Volume of H₂O
0:1 PVA/PVP	0 g	2 g	8 mL
1:1 PVA/PVP	1 g	1 g	8 mL
1:2 PVA/PVP	1 g	2 g	12 mL
2:1 PVA/PVP	2 g	1 g	12 mL
1:3 PVA/PVP	1 g	3 g	16 mL
3:1 PVA/PVP	3 g	1 g	16 mL
1:0 PVA/PVP	2 g	0 g	8 mL

The protocols for preparing the solutions were adapted from the literature [1][19]. As performed in the literature, the solutions were heated to 90°C in a 50-mL tube and periodically vortexed to ensure complete mixing of the polymer solutions [19].

The solution of 0:1 PVA/PVP matrix polymer solution was created through the combination of 4 grams of PVP and 4 mL of water in the case of 50% by mass and 2 grams of PVP with 8 mL of water in the case of 20% by mass. The 1:1 PVA/PVP matrix polymer solution was made through the combination of 2 grams of PVP, 2 grams of PVA, and 4 mL of water in the case of 50% by mass and 1 gram of PVP, 1 gram of PVA, and 8 mL of water in the case of 20% by mass. The 1:2 PVA/PVP matrix polymer solution was created through the combination of 1 gram of PVA, 2 grams of PVP, and 3 mL of water in the case of 50% by mass and 1 gram of PVA, 2 grams of PVP, and 12 mL of water in the case of 20% by mass. The 2:1 PVA/PVP matrix polymer solution was created through the combination of 2 grams of PVA, 1 gram of PVP, and 3 mL of water in the case of 50% by mass and 2 grams of PVA, 1 gram of PVP, and 12 mL of water in the case of 20% by mass. The 1:3 PVA/PVP matrix polymer solution was created through the combination of 1 gram of PVA, 3 grams of PVP, and 4 mL of water in the case of 50% by mass and 1

gram of PVA, 3 grams of PVP, and 16 mL of water in the case of 20% by mass. The 3:1 PVA/PVP matrix polymer solution was created through the combination of 3 grams of PVA, 1 gram of PVP, and 4 mL of water in the case of 50% by mass and 3 grams of PVA, 1 gram of PVP, and 16 mL of water in the case of 20% by mass. Finally, the 1:0 PVA/PVP solution was created through the combination of 4 grams of PVA and 4 mL of water in the case of 50% by mass and 2 grams of PVA and 8 mL of water in the case of 20% by mass. To ensure consistency, all solutions were heated for 4 hours at 90°C and periodically vortexed to ensure thorough mixing. The resultant mixtures were incubated overnight at 37°C.

2.1.3 Casting Matrix Polymer in Microneedle Molds

The general protocol used for casting the polymer into the microneedle molds was adapted from the literature with modifications [1][19]. Throughout the course of the project, several methods of casting matrix polymer were developed and refined. Ultimately, 5 μ L of 20% by mass polymer solution blended with 5 μ L of the target protein drug solution were mixed together and cast in the microneedle mold. The molds were allowed to dry within a desiccator at 4°C for two days or until fully dry. A microneedle mold containing a blend of 3:1 PVA/PVP in the drying process is displayed in Figure 6.

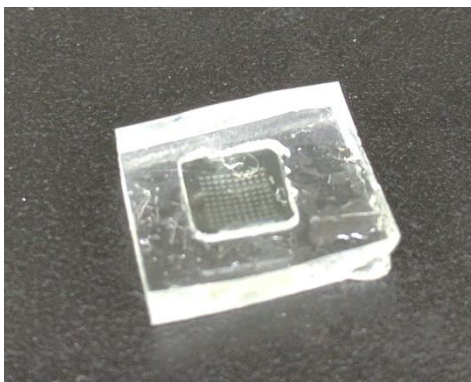


Figure 6. PDMS Mold containing 3:1 PVA/PVP polymer solution.

2.1.4 Model Protein Encapsulation in Microneedle

In order to evaluate the feasibility of protein drug delivery through the skin via the application of a microneedle patch, the model protein bovine serum albumin (BSA) was encapsulated within the matrix polymer solution. 20 μL of BSA solution of various concentrations (ThermoFisher Scientific, Waltham, MA) and 10 μL of 20% by mass matrix polymer solution were added to a 300 μL conical tube and mixed thoroughly. 20 μL of water was mixed in the case of the control. 5 μL of this mixed solution was then added to the microneedle mold matrix. The mold was placed in a desiccator to dry.

2.1.5 Model Protein Fluorescence Labelling

To facilitate the identification of model protein diffusion, the DyLight™ 650 NHS Ester was conjugated to BSA at primary amine sites. 50 μg of DyLight™ 650 NHS Ester (ThermoFisher Scientific, Waltham, MA) was suspended in 20 μL of anhydrous dimethyl sulfoxide (DMSO). 6 μL of this mixture was combined with 100 μL of BSA and mixed using a thermomixer (Thermomixer R, Eppendorf, Hauppauge, NY) at a temperature of 25°C and a speed of 1000 rpm for a duration of 4 hours. The combined solution was filtered using a microcentrifuge filter with a 10 kDa cutoff. After a 10-minute period of filtering at 14g, the concentrate was collected by inverting the filtration unit and centrifuging at 2000g for 2 minutes. The concentrate was assayed for fluorescence intensity using a fluorospectrometer (NanoDrop 3300, ThermoFisher Scientific, Waltham, MA) and resuspended in PBS to reach a final volume of 100 μL . This process was repeated until zero fluorescence intensity was detected in the range of the 650nm from the filtrate waste.

2.1.6 VEGF Protein Encapsulation in Microneedle

In order to encapsulate VEGF in the microneedle array, a similar protocol to the model drug encapsulation was developed. 5 μL of 20% by mass matrix solution and 5 μL of 10 $\mu\text{g}/\text{mL}$ (total of 50 ng) VEGF solution were mixed and added to each microneedle mold. 50 ng was loaded into each microneedle to represent an excess of established biomaterial delivery of VEGF for proof of concept [20], [21].

2.2 Mechanical Performance Evaluation

The mechanical performance of microneedle arrays was evaluated using an axial compression machine (Instron 5960, Norwood, MA). A 10N load cell and compression rate of 0.5 mm/s was used to determine the stress/strain relationship of the microneedle array via Bluehill® software. The load force as a function of displacement distance was obtained and plotted. Points of discontinuity or plateau were interpreted as the location of mechanical failure. The load force at this extension distance was taken to be the maximum force tolerable by the microneedle array. The average fracture force per needle was calculated from the maximum fracture force divided by the total number of needles in the microneedle array affected.

2.3 Protein Drug Tertiary Structure Evaluation

Fluorescence spectroscopy was utilized to evaluate the tertiary structure of the model protein BSA before and after microneedle encapsulation using a procedure adapted from the literature [22]. 6 samples were scanned for intrinsic fluorescence: stock phosphate-buffered saline (PBS), stock BSA in PBS, dissolved BSA encapsulated microneedle, dissolved blank microneedle, stock BSA in PBS heated

to 80°C for 30 minutes, stock BSA in PBS brought to pH 2 using hydrochloric acid. 100 µL of each sample was loaded onto a Greiner 96-well plate. Using a plate reader (Tecan Infinite® 200 Pro, Switzerland), the 96-well plate was rocked for 10 seconds and a fluorescence intensity scan was performed using a fixed excitation wavelength of 280 nm and emission spectra range of 300-400 nm. All resulting values were normalized to the PBS buffer. The resulting fluorescence intensity as a function of wavelength plots were analyzed in comparison to the controls.

2.4 Model Drug Release Efficiency Evaluation

The efficiency of release of the model protein BSA was evaluated through the quantification of BSA dissolved from the microneedle as compared to the known quantity encapsulated. A fluorescently-labeled BSA encapsulated microneedle was dissolved in 1 mL of PBS and evaluated using a fluorospectrometer (NanoDrop 3300, ThermoFisher Scientific, Waltham, MA). Through the use of a standard curve generated using an equal volume of a known concentration of fluorescently-labeled BSA, an approximate concentration was quantified through interpolation. The quantified BSA was compared to the known encapsulation quantity to determine a release efficiency proportion.

2.5 In-Vitro Insertion Testing

The ability of fabricated microneedle arrays to penetrate the skin and deliver their payload was evaluated through *in-vitro* insertion testing using sacrificed mice. All hair on the backs of mice were removed through shaving and the use of a depilatory cream. Using the spring-loaded applicator device (Micropoint Technologies, Singapore) pictured below in Figure 7, the microneedle array loaded with fluorescently-labeled BSA was applied to the exposed skin. After allowing the drug payload to diffuse

into the skin for 5 minutes, the applicator was removed and the region of skin was excised. The depth and overall distribution of fluorescence in the skin sample was then evaluated using a confocal microscope (Olympus Fluoview 1000, Center Valley, PA). A z-stack was obtained and evaluated to determine the maximum depth of fluorescence identification within the sample. The skin sample was also sliced into 20 μm sections through the use of a cryostat device (Leica CM1950, Buffalo Grove, IL) and analyzed for fluorescence and indications of skin puncture using an in-vivo imaging system (CRi Maestro, Woburn, MA).



Figure 7. Microneedle Applicator Device

2.6 Enzyme-linked Immunosorbent Assay (ELISA)

In order to quantify the encapsulation efficiency of VEGF, a sandwich type enzyme-linked immunosorbent assay (ELISA) (PeproTech, Rocky Hill, NJ) was performed. The manufacturer protocol and instructions were followed and are briefly summarized here. Rabbit Anti-Human VEGF capture antibody was seeded and block buffer to minimize non-specific binding. Standards and samples were diluted and added in triplicate. Biotinylated Rabbit Anti-Human VEGF detection antibody was used to

bind present VEGF. Avidin-HRP conjugate was added, followed by ABTS substrate to promote color development based on detected VEGF. A plate reader (Tecan Infinite® 200 Pro, Switzerland) was used to quantify color development.

2.7 In-Vitro Endothelial Cell Tube Formation Assay

In order to evaluate the functionality of encapsulated VEGF, a standard endothelial cell tube formation assay with slight modifications was conducted [23]. Polymeric microneedles containing encapsulated VEGF were dissolved in 0.2 mL of water. Using a standard 24-well plate, 160 μ L of thawed Geltrex™ reduced growth factor basement membrane matrix (ThermoFisher Scientific, Waltham, MA) was added to each well and the plate was incubated at 37°C for 24 hours. 1 mL of dPBS was added to each well and the plate was incubated at 37°C for 24 hours, after which the dPBS was removed in order to reduce soluble growth factor interference. Human Umbilical Vein Endothelial Cells (HUVECs) between passage 2 and 7 were selected for use in this assay. The HUVEC cells were cultured in media lacking Low Serum Growth Supplement (LSGS) for 12 hours. Cells were detached from the culture flask using 5mL of 0.05% Trypsin/EDTA (ThermoFisher Scientific, Waltham, MA) and incubated for roughly 2 minutes or until cells were visibly round. 5 mL of M200 media supplemented with 0.5% fetal bovine serum (FBS) were added to the flask and all contents were centrifuged at 0.2 RCF for 5 minutes. The supernatant was removed and cells were resuspended in 1mL of M200 media supplemented with 0.5% FBS. Using a hemocytometer, a cell count was obtained within a known volume of media to determine an approximate cell density. After adding approximately 80,000 cells to each well, the plate was incubated for 30 minutes, after which the media was replaced. The appropriate microneedle VEGF samples was added to each well. Remaining cells were added to a T75 flask with 10 mL of M200 media supplemented with low serum growth supplement (LSGS). After 6 hours, the wells were stained with Calcein AM (final

concentration of 2 $\mu\text{g}/\text{mL}$) and incubated 30 min at 37 $^{\circ}\text{C}$. The formation of tubes was then observed under a microscope.

2.8 In-Vitro Endothelial Cell Proliferation Assay

The bioactivity of microneedle encapsulated VEGF was evaluated through an endothelial cell proliferation assay. Polymeric microneedles containing encapsulated VEGF were dissolved in 0.2 mL of M200 media supplemented with 0.5% FBS. A 96-well plate was coated with a solution of 0.1% gelatin solution and incubated for 10 minutes before the gelatin was removed. A similar cell culture passaging procedure was performed as in section 2.7. The HUVEC cells were cultured in media lacking Low Serum Growth Supplement (LSGS) for 12 hours. After adding approximately 10,000 cells to each well of a 96-well plate, prescribed quantities of dissolved VEGF-containing microneedles (10 ng/mL, 20ng/mL) and stock VEGF (10 ng/mL, 0 ng/mL) were added to the appropriate wells and the cells were allowed to proliferate under incubation for two-three days. In order to assay proliferation, 20 μL of CellTiter 96 reagent was added to each well and the absorbance at 490 nm was recorded every hour for four hours using an ELISA plate reader (Tecan Infinite[®] 200 Pro, Switzerland).

2.9 In-Vitro Integrated Cell Proliferation Assay

In order to evaluate the functional microneedle delivery of VEGF through a realistic tissue mimic, an integrated cell proliferation assay was carried out similar to that described in 2.8. Polymer microneedles containing 50 ng VEGF were fabricated. An 2.6% agarose skin phantom was created to mimic the skin's viscoelasticity by mixing 0.26g agarose gel in a total volume of 10 mL 1X PBS [24]. The experimental groups included a blank (culture media only), a negative control (0ng VEGF), a

positive control (50 ng VEGF), a microneedle group containing 50ng VEGF, and a microneedle group containing 0ng VEGF. All experimental groups were performed in triplicate.

A standard cell culture procedure was performed as described in 2.7 with slight modifications. A 24-well cell culture dish was pre-treated with a solution of 0.1% gelatin solution and incubated for 10 minutes before the gelatin was removed. The HUVEC cells were cultured in media lacking Low Serum Growth Supplement (LSGS) for 12 hours. After the establishment of an overall cell concentration, the HUVEC cell culture solution was diluted to 100 cells/ μL and seeded in a 24-well plate with a volume of 400 μL to achieve a total of 40,000 cells/well (~20% confluency). 500 μL of M200 media supplemented with 0.5% FBS and 1% antibiotic was added to each experimental group. The positive control cell culture media was infused with 50 μL of 1 $\mu\text{g}/\text{mL}$ VEGF for a total 50 ng.

Polymer microneedles were inserted into agarose disks and were allowed to dissolve for 5 minutes before the base was removed from the tissue phantom. The tissue phantom slices were then inserted into transwells and placed in their respective wells. After 2 days of cell growth and proliferation, 100 μL of CellTiter 96 reagent was added to each well and the absorbance at 490nm and 650nm was quantified using an ELISA plate reader (Tecan Infinite® 200 Pro, Switzerland) four hours post infusion.

2.10 In-Vivo Assay

In order to determine the efficacy of VEGF functionalized microneedle arrays outside of a controlled environment and within complex, live biological systems, an *in-vivo* assay was performed using standard laboratory mice. Sterile microneedles were inserted into the backs of the mice in the arrangement shown in Figure 8. The manufacturing procedure for VEGF microneedles was modified slightly by conducting all procedures within the sterile cell culture fume hood environment to ensure sterility of the microneedles.

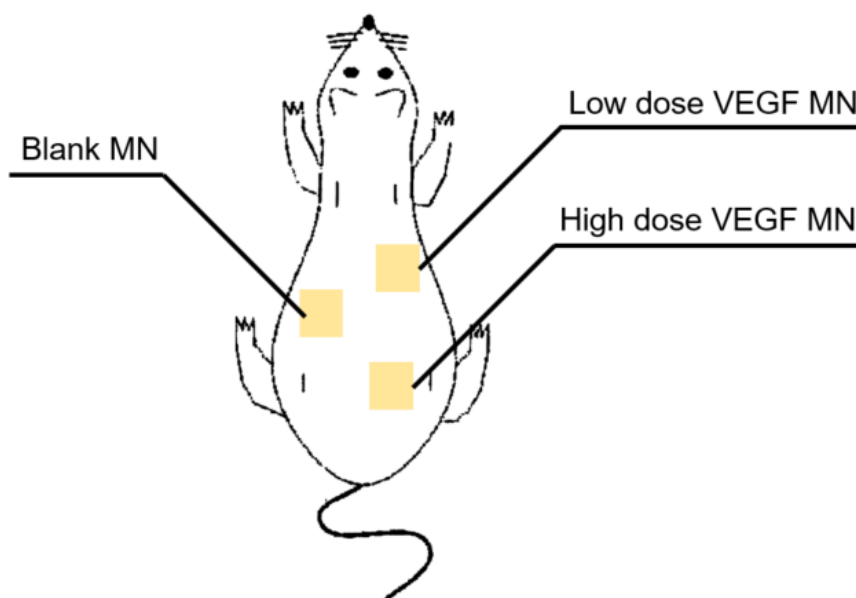


Figure 8. Schematic of MN Insertion Sites.

The tests were conducted under an Institutional Animal Care and Use Committee (IACUC) approved protocol. Standard laboratory female mice were anesthetized using Isoflurane and their backs were shaved of all hair. A depilatory cream, Nair™, was applied to remove excess hair. After removal of cream, the mice were allowed to recover for a period of 24 hours. After recovery, the mice were placed under anesthesia and three microneedles were inserted on the dorsal region in the arrangement shown in Figure 8. The three microneedles included one control and two experimental groups – a high dose (500 ng) and low dose (50 ng) of VEGF and were secured using Tegaderm™ for 30 minutes to allow the microneedles to dissolve into the skin. At the conclusion of the application period, the microneedles were removed from the skin and both the microneedle tips and the dorsal region of the mice were imaged. Each day for a period of seven days, the mice were visually evaluated for well-being and overt signs of inflammation or erythema on the dorsal region. Images were captured of the dorsal region over the 7-day period.

2.11 Statistical Analysis

Quantitative data are expressed as mean \pm sample standard deviation from the mean. Comparison between groups was accomplished through a student's t-test ($\alpha = 0.05$) and one-way analysis of variance (ANOVA) ($\alpha = 0.05$) in the case of two groups or multiple groups respectively. All results were considered statistically significant with p-values < 0.05 .

Chapter 3

Results and Discussion

3.1 Summary of Results

This study demonstrated the successful fabrication of polymeric microneedles capable of delivering a bioactive drug payload through the skin. *In-vitro* studies have shown successful encapsulation of VEGF into microneedles and suitable bioactivity. Ongoing research efforts are aimed at successfully delivering a therapeutic dose of VEGF *in-vivo*.

3.2 Microneedle Fabrication

In this study, microneedles were designed with the primary goal of successfully piercing the stratum corneum skin layer and delivering a bolus of bioactive VEGF to the tissues. This was accomplished by designing a microneedle array constructed from the strong, water-soluble polymers PVP and PVA. Proteins of interest were incorporated directly into the aqueous polymer blend and cast onto PDMS microneedle molds. The resulting microneedles were characterized physically through scanning electron microscopy (SEM), brightfield microscopy, and fluorescence microscopy as shown in Figures 9-11. The microneedle arrays consisted of 100 (10 x 10) pyramidal micro-scale needles with a base, height, and tip-to-tip distance of 200 μm , 600 μm , and 500 μm , respectfully.

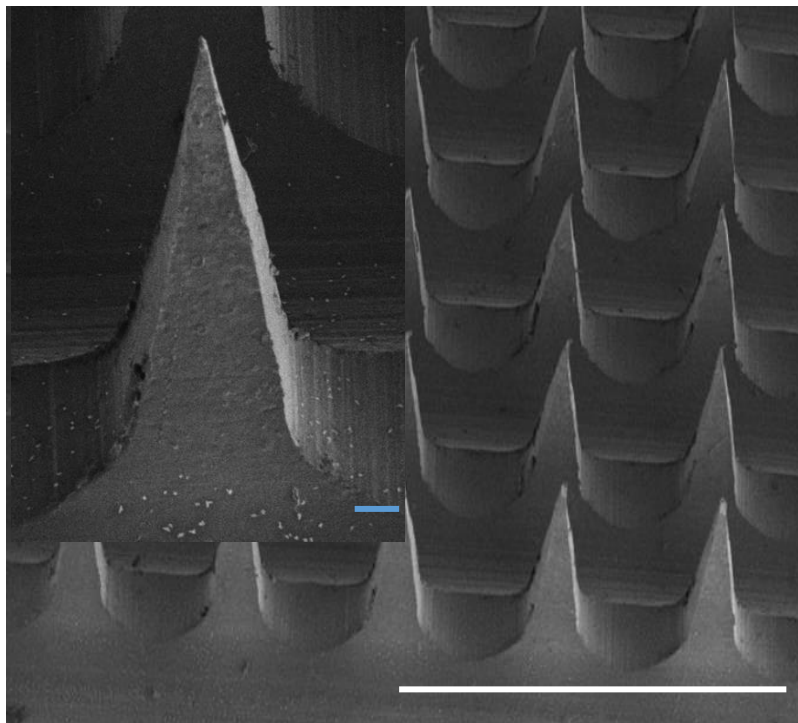


Figure 9. SEM image of Microneedle Array. Scale bar: 1mm. Insert scale bar: 100µm.

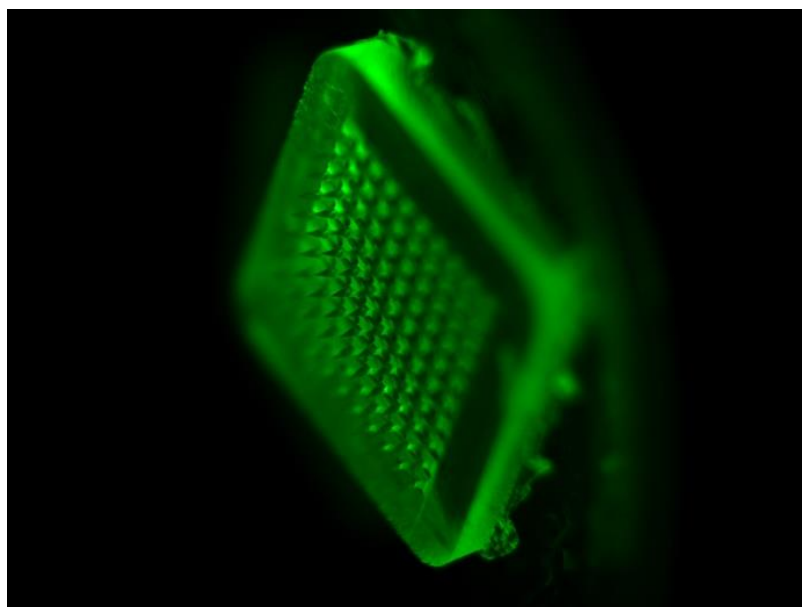


Figure 10. Representative Microneedle Arrays.

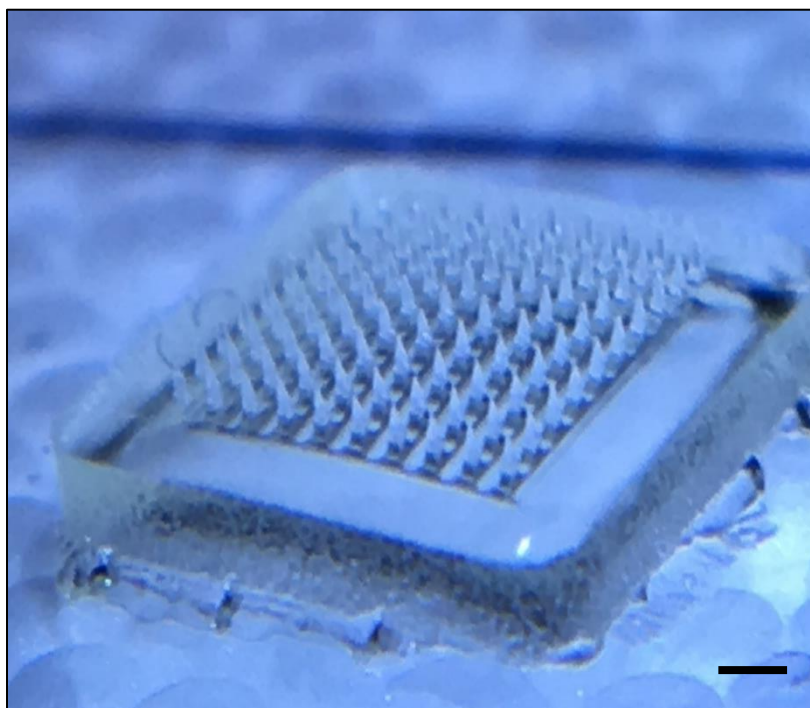


Figure 11. Representative Microneedle Array. Scale bar: 1mm

3.3 Microneedle Mechanical Performance

Before assessing mechanical strength for purposes of skin penetration, solutions containing various ratios of PVA and PVP were evaluated to determine the ideal polymer combination for continuing study. The ideal blend of PVP and PVA polymers to create the mechanical strength necessary was largely determined through mechanical performance evaluation. The resulting fracture force from the respective PVP/PVA polymer blends are compared in Figure 12. It was found that no significant difference in fracture force was observed in the polymer blends tested, so the polymer blend of 3:1 PVA/PVP was selected for further testing due to its prevalence in the literature [25]. It is thought that no significant difference was observed due to the reasonable variation in force measured from each individual microneedle, resulting in a large standard deviation.

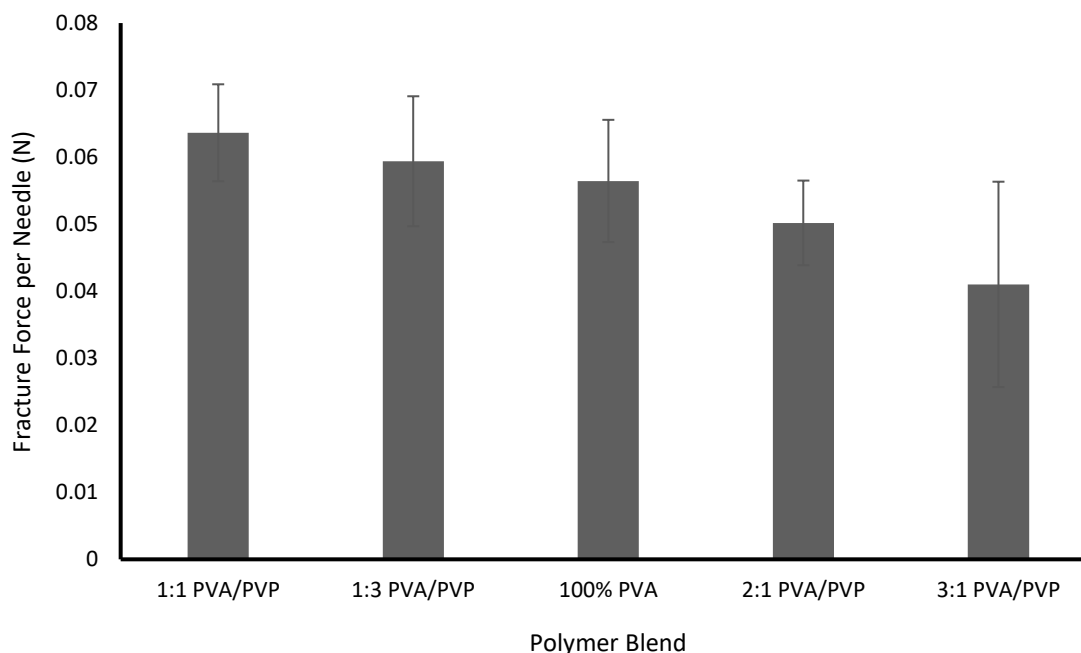


Figure 12. Fracture Force per Needle of Various MN Polymer Combinations. Each result is the mean of 3 samples. The error bars represent ± 1 standard deviation from the reported mean. No statistically significant differences were observed.

In order to determine if the fabricated microneedles were capable of penetrating the skin, the critical mechanical/material properties of the needles were determined through the use of an axial compression instrument as described previously. In addition to a stress-strain curve characteristic of microneedle polymer performance, a plot of force as a function of compression head extension was computed to determine the peak mechanical load before failure. Also of interest was the impact of protein encapsulation on mechanical strength. The mechanical strength of polymer microneedles with no protein encapsulated as well as microneedles containing the model protein BSA was evaluated. A representative force versus extension plot is shown in Figure 13 while the measured fracture force per needle for both control microneedles and BSA loaded microneedles is displayed in Figure 14.

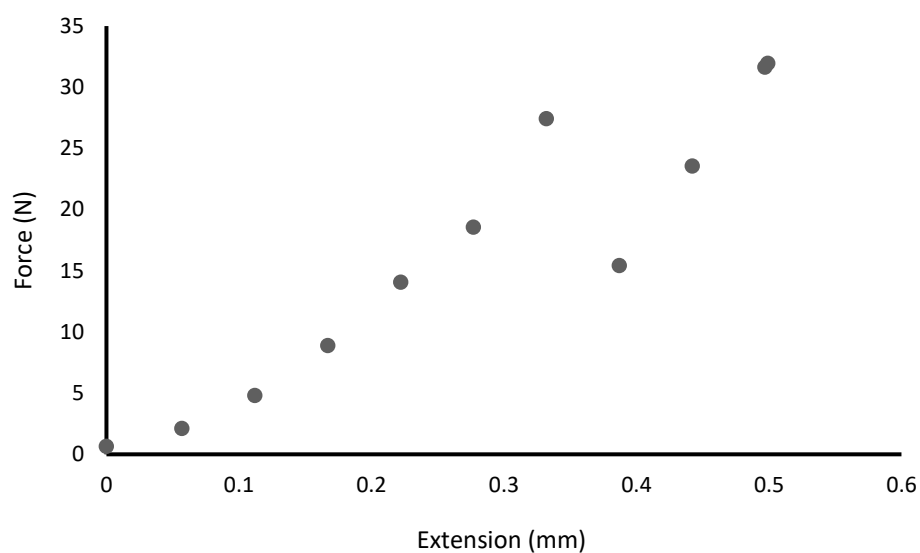


Figure 13. Representative Force vs Extension Plot. 3:1 PVA/PVP Microneedles used for evaluation. The sharp depression observed at 27N is taken to be the fracture point.

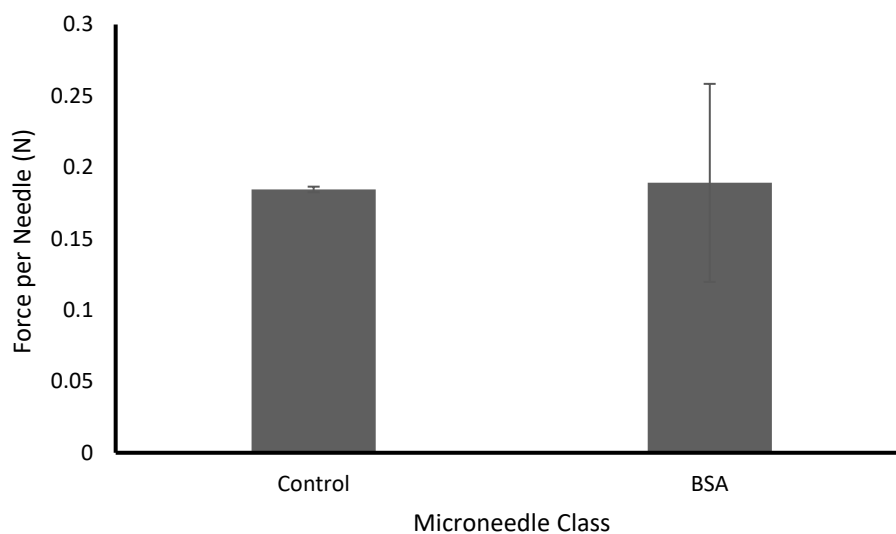


Figure 14. Mechanical Strength of Protein Encapsulated Microneedles. Each result is the mean of 3 samples. The error bars represent ± 1 standard deviation from the reported mean. No statistically significant differences were observed.

As evident from Figure 14, there is no statistically significant difference in the peak force observed in control microneedles and microneedles loaded with the model protein BSA. As reported in the literature, an insertion force of 0.058 N/needle was found to be necessary to penetrate the skin using microneedle systems of similar characteristics [26]. From the results shown in Figure 14, both control and BSA microneedles meet these criteria. These results support the theory that the incorporation of proteins into the polymer microneedle matrix does not measurably impact the strength of the microneedles, and therefore should not demonstrate lower performance in skin insertion testing. The relatively large variation observed in BSA microneedle testing confounds the result slightly, however even 1 standard deviation below the mean results in a fracture force above that needed to penetrate the skin. Based on reported literature and the obtained mechanical force data, the microneedles appear to be of sufficient strength to penetrate the skin.

3.4 Protein Tertiary Structure Assessment

In order to assess the tertiary structure of proteins loaded into the polymer microneedles, the model protein BSA was used due to the relatively low cost involved in using a large amount to enable the use of fluorescence spectroscopy. Three amino acids contain intrinsic fluorescence properties (Phe, Tyr, and Trp) that are excited at 280 nm and whose properties are extremely sensitive to their environment that varies depending on the folding state of the protein [27], [28]. As a result, by analyzing the fluorescence emission spectra, one can determine if a significant portion of the protein sample has lost its tertiary conformation, and therefore also its biological activity. Figure 15 displays a fluorescence emission spectra of stock BSA, controls of denatured BSA, a blank microneedle control, as well as microneedle samples containing BSA. As is evident from the curves displayed in Figure 15, the stock BSA curve and the BSA

microneedle curves follow the same general fluorescence pattern while the denatured BSA samples are skewed. There was minimal to no fluorescence activity in the microneedle control trial.

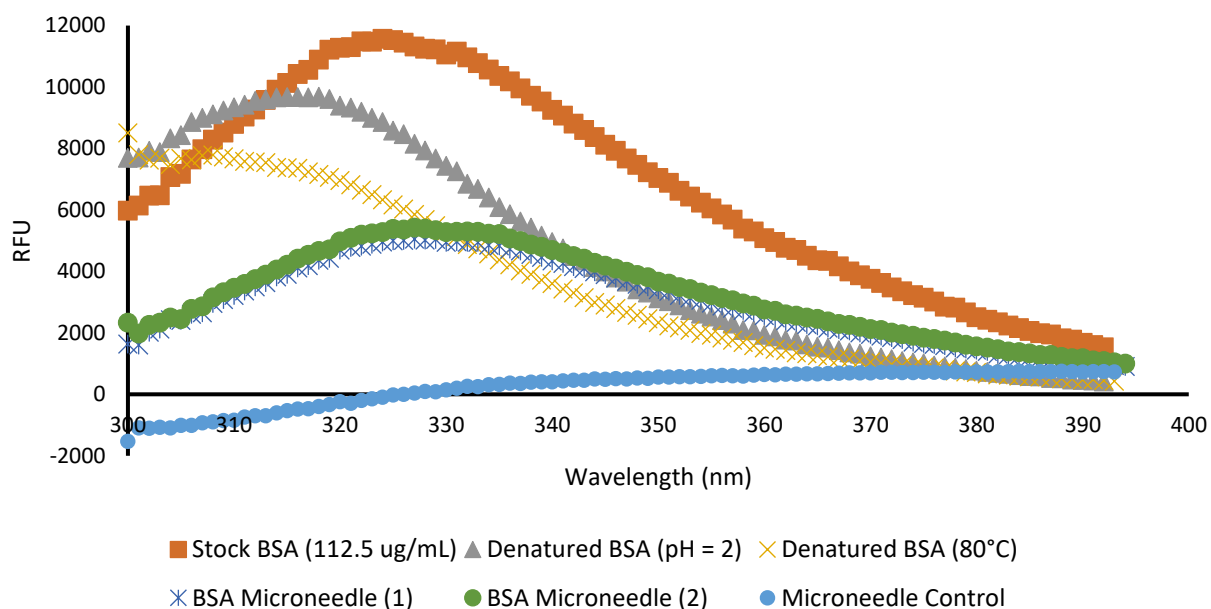


Figure 15. BSA Fluorescence Intensity Assay. Excitation wavelength was 280 nm; emission measured from 300 to 400 nm. Denatured BSA reflects a different emission pattern compared to stock BSA and microneedle sample BSA.

The hydrophobic amino acids Trp, Tyr, and Phe are located on the interior of the folded protein due to their hydrophobic nature and follow the characteristic fluorescence pattern shown from the stock BSA curve. Since the BSA microneedle samples were observed to follow the same fluorescence pattern, it is reasonable to conclude that the bulk of the BSA encapsulated within the microneedles maintained its folded tertiary structure. While the overall fluorescence pattern was observed to be similar between the stock BSA trial and the BSA microneedle trials, the relative fluorescence intensity of the BSA microneedle trials was markedly lower, suggesting a portion of the original encapsulated BSA was undetected. Further experimentation suggested that the PVA/PVP polymer may block the fluorescence signal of BSA. As shown in Figure 16, a similar emission spectra pattern was observed for BSA with and

without the addition of PVA/PVP polymer with the exception of fluorescence intensity magnitude. The fluorescence spectra obtained supports the conclusion that the tertiary structure of bulk BSA encapsulated is unaltered, however the lower fluorescence intensity observed among the BSA microneedle samples suggests that a significant portion of BSA was shielded by the polymer.

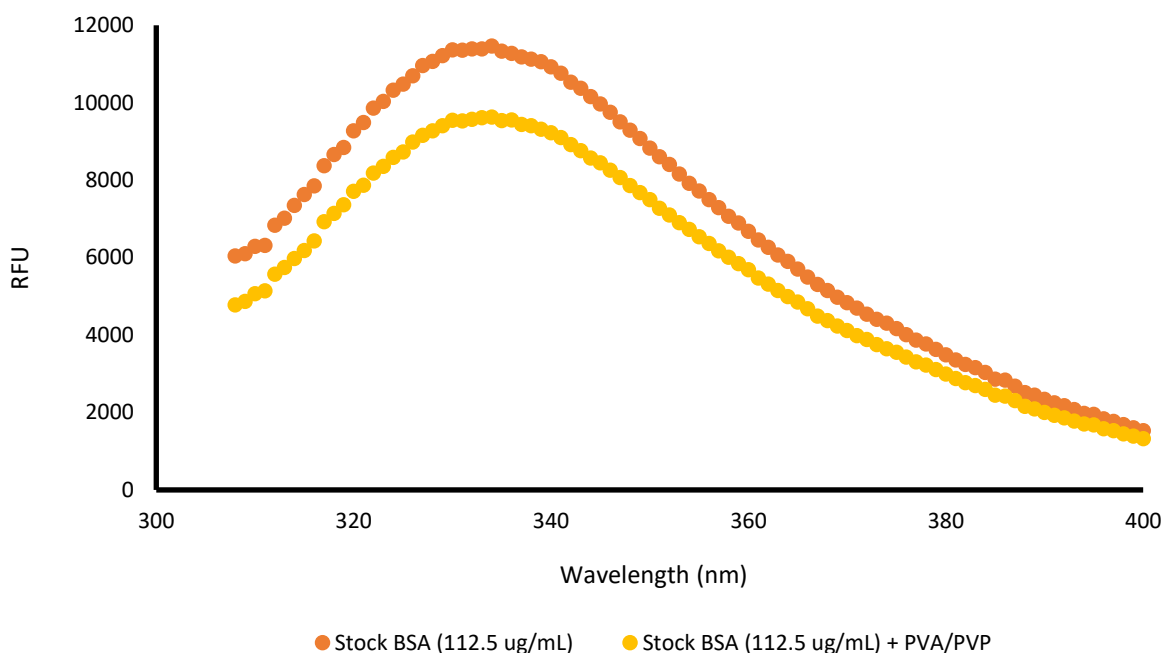


Figure 16. BSA Fluorescence Intensity with/without PVA/PVP. The emission pattern appears similar, however the intensity magnitude of the curve associated with BSA mixed with polymer is depressed.

3.5 In-Vitro Insertion Assessment

In order to determine if the polymer microneedles that were manufactured were capable of penetrating skin, an *in-vitro* model of freshly euthanized mouse skin was used. Fluorescently tagged BSA was encapsulated into the tips of the polymer microneedles in order to detect insertion distance and analyze insertion patterns.

Figure 17 shows fluorescently labeled BSA localized to the tip region of polymer microneedles prior to insertion into mouse skin. Figure 18 shows the maximum insertion depth achieved from polymer microneedle penetration into a cryo-sectioned slice of mouse skin via fluorescent markers.

Based on the demonstrated visual evidence of fluorescently labeled BSA delivered below to depths that surpass the stratum corneum skin layer, it was concluded that the fabricated polymer microneedles possess sufficient mechanical strength to penetrate the skin.

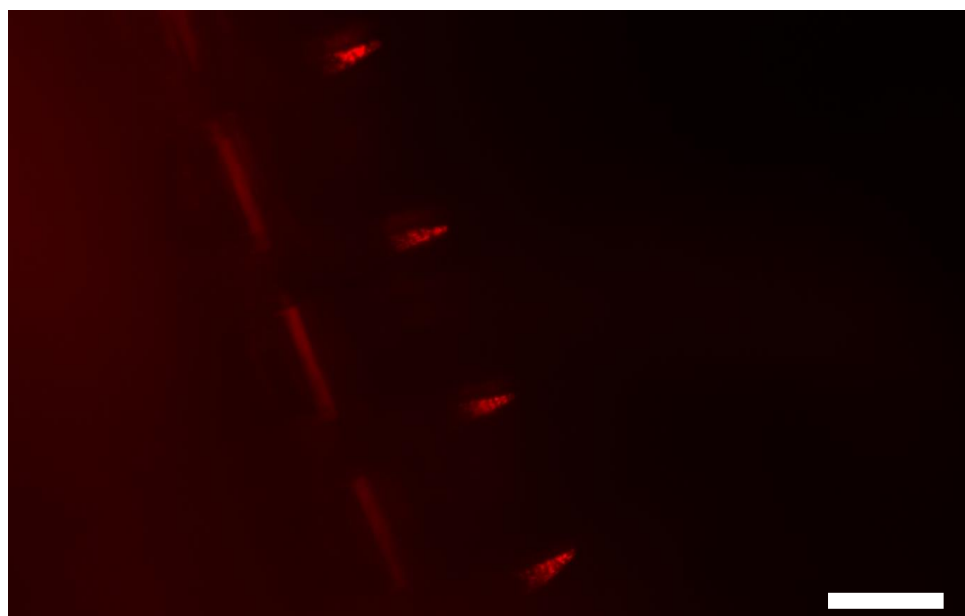


Figure 17. Fluorescently Tagged BSA Isolated to Tip-Region within Microneedle Array.
Scale bar: 200 μm .

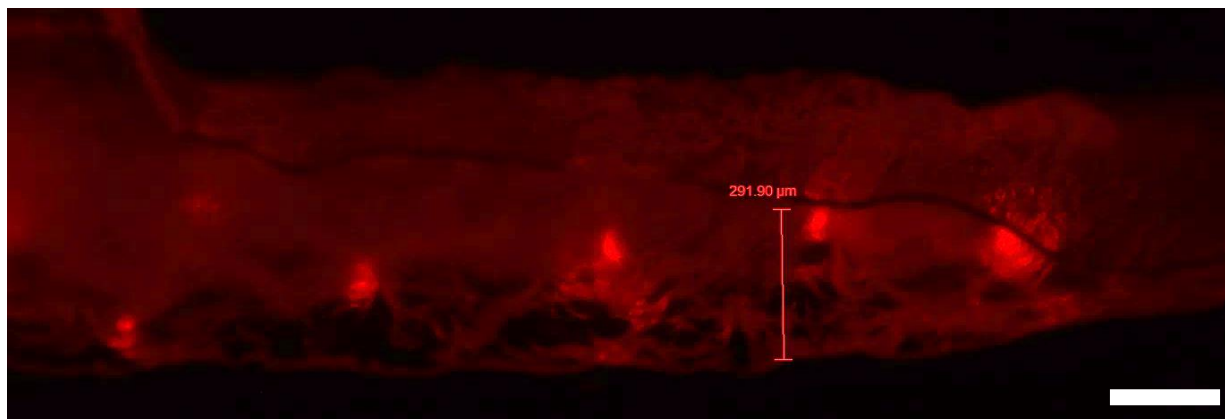


Figure 18. Cross-section of Mouse Skin showing maximum insertion depth. Scale bar: 200 μm .

3.6 Protein Release Efficiency

In order to determine the efficacy of growth factor release from polymer microneedles, an enzyme linked immunosorbent assay was performed as a means to quantify the VEGF released into solution. All microneedles were loaded with 50ng of VEGF during the fabrication process. The quantified levels of VEGF after encapsulation and dissolution in addition to the computed release efficiency are displayed in Table 3. A student's t-test was performed to compare the VEGF release ability between the two microneedle classes: 3:1 PVA/PVP with sucrose and 3:1 PVA/PVP without sucrose. The two groups were not determined to be statistically different ($p = 0.47$), therefore sucrose as a stabilizing polysaccharide additive was not deemed to improve release efficiency.

Table 3. ELISA Detected VEGF Release Efficiency

Microneedle Class	Mean VEGF Detected (ng)	Standard Deviation (ng)	Mean Release Efficiency (%)
3:1 PVA/PVP	45.6	5.97	91
3:1:1 PVA/PVP/Sucrose	52.7	9.44	100

It is thought that due to the detection method of ELISA and its reliance on antibodies to bind to unique epitopes on the VEGF protein molecule that there was reasonable evidence to support the presence of VEGF. There is not enough evidence from ELISA to support the presence of bioactive VEGF.

3.7 In-Vitro Protein Bioactivity Assessment

In order to gauge the bioactivity of the growth factor post-encapsulation in polymer microneedles, a series of *in-vitro* endothelial cell assays were performed. Over the course of experimentation, the endothelial cell tube formation assay and the endothelial cell proliferation assay were performed using HUVECs.

The endothelial cell tube formation assay successfully demonstrated bioactive VEGF. The assay was performed using a positive control of standard VEGF (10ng/mL), a negative control (0 ng/mL), as well as varying VEGF concentrations of dissolved microneedle samples in triplicate. Tube lengths were qualitatively compared to the control groups for significance. The positive control and negative control revealed tube formation as expected. Microneedle samples containing 10 ng/mL VEGF generally displayed moderate tube formation. Microneedles containing 20 ng/mL VEGF displayed some tube formation and evidence of proliferation with large quantities of cells visible in the images. Microneedles containing 40 ng/mL contained limited tube formation and extensive evidence of proliferation with large masses of cells present in the sample wells. Figures 19-23 display representative examples of the controls as well as the experimental conditions. While the results are not suggestive of a direct relationship between VEGF dose and tube formation, there was convincing evidence suggesting that the VEGF encapsulated within the microneedles displayed adequate bioactivity to induce the formation of new blood vessels. A secondary assay, the endothelial cell proliferation assay, was performed to further substantiate these observations.

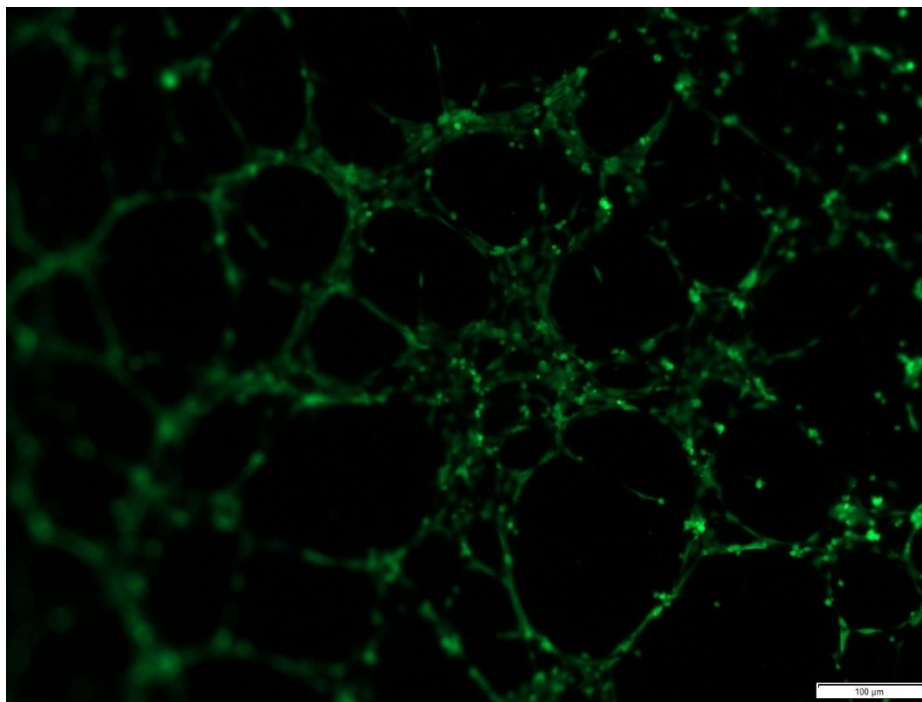


Figure 19. Representative Tube Formation Positive Control. 10 ng/mL stock VEGF solution added to HUVECs. Closed loop tube formation was observed.

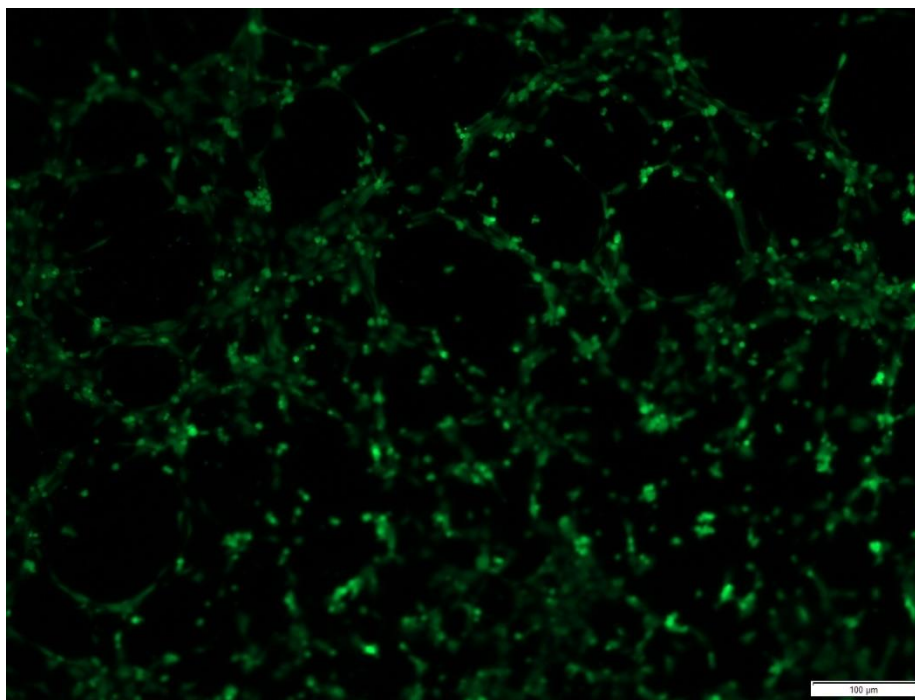


Figure 20. Representative Tube Formation Negative Control. No VEGF was added and limited tube formation was observed.

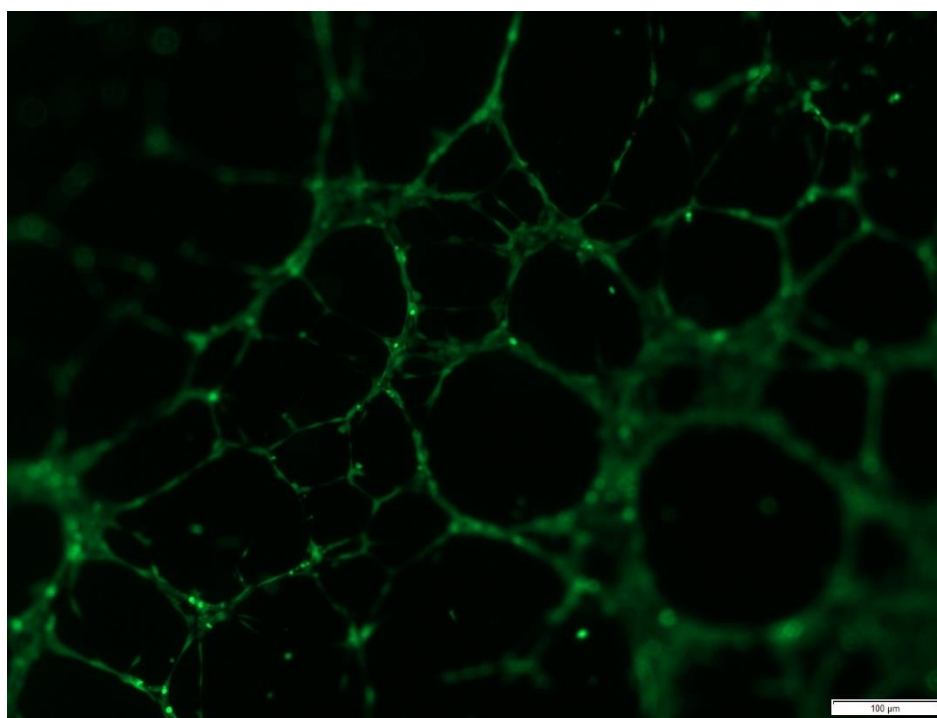


Figure 21. Representative Tube Formation 10 ng/mL VEGF Microneedle. Microneedles containing 10 ng/mL VEGF were dissolved and added to HUVECs. Moderate tube formation was observed.

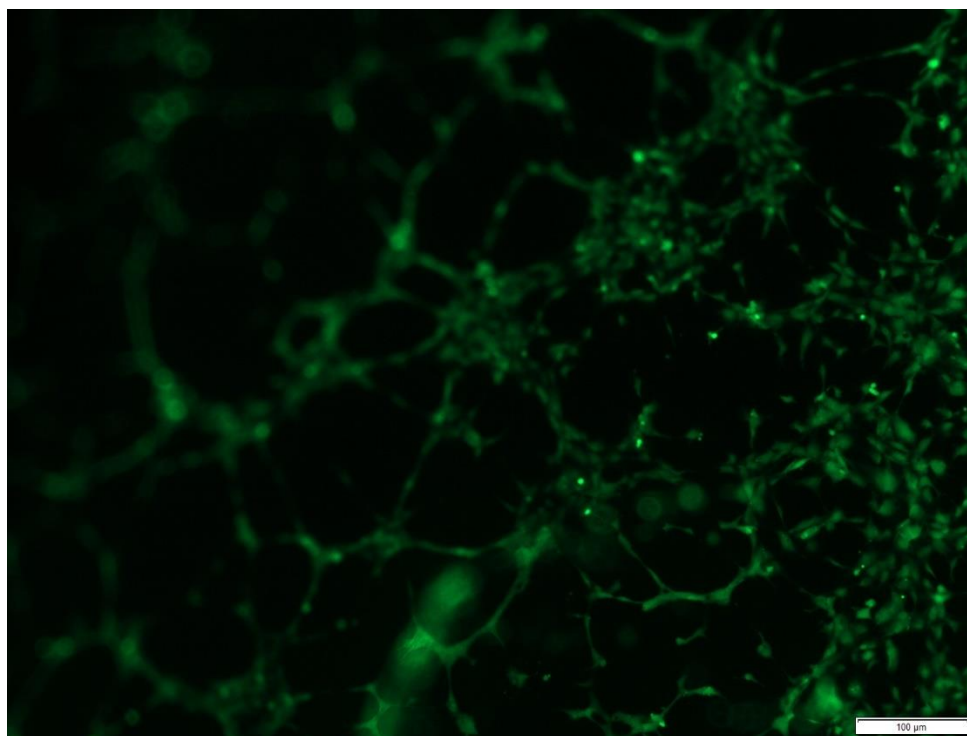


Figure 22. Representative Tube Formation 20 ng/mL VEGF Microneedle. Microneedles containing 20 ng/mL VEGF were dissolved and added to HUVECs. Cell proliferation and limited tube formation were observed.

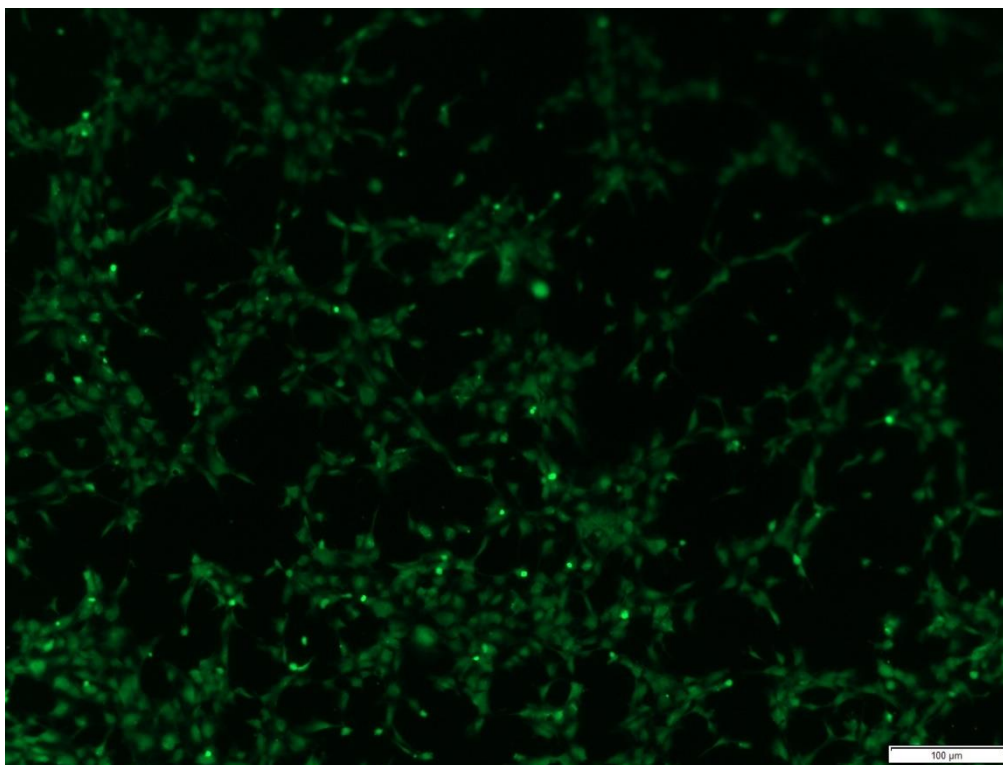


Figure 23. Representative Tube Formation 40 ng/mL VEGF Microneedle. Microneedles containing 40 ng/mL VEGF were dissolved and added to HUVECs. Cell proliferation and limited tube formation were observed.

The endothelial cell proliferation assay was designed to measure the relative proliferative effects of VEGF-encapsulated microneedles. Similar to the endothelial cell tube formation assay, a positive control of standard VEGF (10ng/mL), a negative control (0 ng/mL), as well as varying VEGF concentrations in triplicate were used. Absorbance measurements obtained for each experimental group reveal convincing evidence of the bioactivity of encapsulated VEGF. Figure 24 displays the results of the endothelial cell proliferation assay. The absorbance of the positive control of 10 ng/mL of stock VEGF was found to be different from that of the 0 ng/mL and 10 ng/mL VEGF microneedles which is reasonable considering that some loss of bioactivity was expected as a result of the encapsulation process. Notably, two VEGF encapsulated microneedles were found to be different from the control microneedle

(0 ng/mL MN), suggesting that additional quantities of VEGF encapsulated within the microneedles created a measurable impact on cell proliferation.

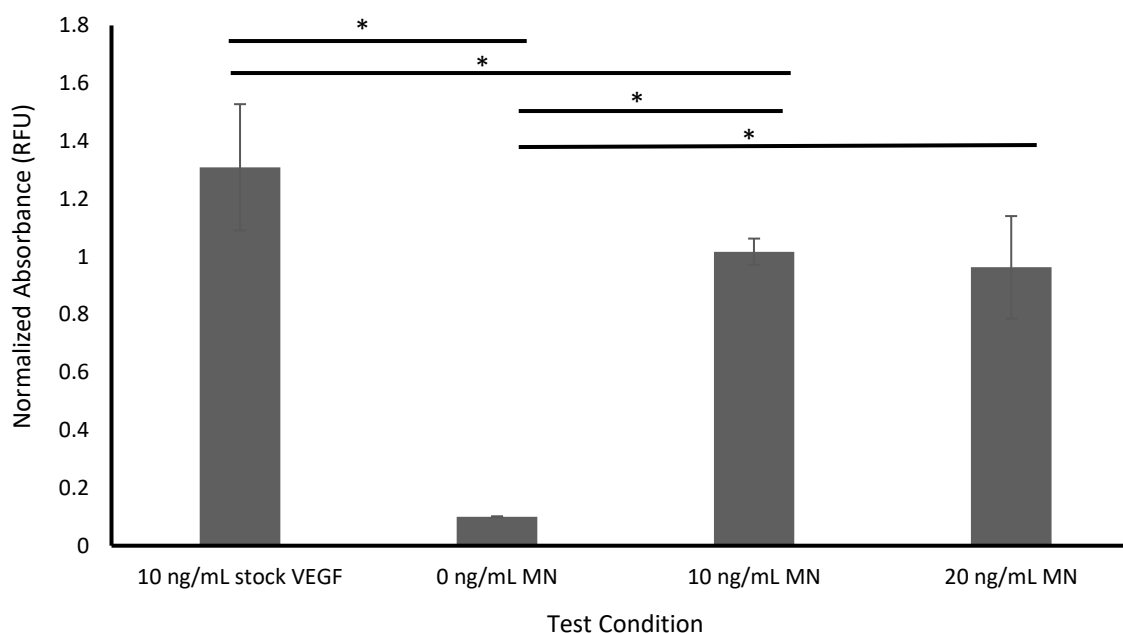


Figure 24. Cell Proliferation Assay. Each result is the mean of 3 samples. The error bars represent ± 1 standard deviation from the reported mean. A single asterisk indicates statistical significance between experimental conditions ($p < 0.05$).

An integrated cell proliferation assay was performed in addition to the standard cell proliferation assay to evaluate microneedle delivery through an agarose-based tissue phantom. Similar to the previous cell proliferation assay, both positive and negative controls were implemented. The positive microneedle experimental groups contained 50 ng VEGF while the negative microneedle experimental groups contained water. The positive control was established at 50 ng VEGF. Figure 25 displays the results of the integrated cell proliferation assay based on normalized absorbance of the proliferation reagent. The results indicate successful delivery of bioactive VEGF protein through an agarose-based skin phantom. Significant differences were established between the controls, the negative control and positive MN, the negative MN and positive MN, and the positive MN and positive control. It was observed that the positive

MN samples were significantly different from both the negative MN samples and the negative control samples, suggesting that the VEGF-encapsulating polymer microneedles were capable of delivering a bolus dose of VEGF through a tissue phantom to influence the proliferation of cultured HUVEC cells.

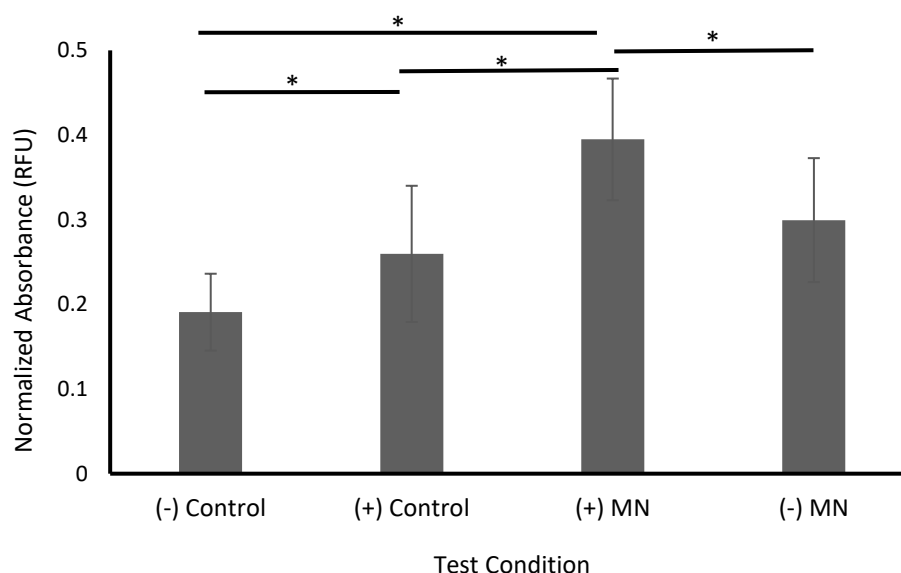


Figure 25. Integrated Cell Proliferation Assay. Each result is the mean of at least 6 samples. The error bars represent ± 1 standard deviation from the reported mean. A single asterisk indicates statistical significance between experimental conditions ($p < 0.05$).

This data reports the mean and standard deviation of three isolated and independent cell proliferation assay events. As expected, the two controls were found to be significantly different from each other. A significant difference was observed between the positive control and the positive microneedle, with the positive microneedle showing increased proliferation relative to the positive control. Additionally, the negative microneedle was not shown to be significantly different from the negative control but a slight increase in absorbance was observed. These unexpected observations have raised the possibility of the PVA/PVP polymer playing a previously unknown enhancement role in overall cell proliferation. Additional study is required to fully elucidate the role of the PVA/PVP polymer

in the cell proliferation assay. Ultimately, the VEGF encapsulating microneedles were deemed capable of delivering a dose of VEGF with sufficient bioactivity to influence the proliferation of HUVEC cells relative to the controls.

Taken together, the results of the endothelial cell tube formation assays and proliferation assay suggest reasonable bioactivity of VEGF post encapsulation in the microneedle polymeric matrix. The tube formation assay indicated that microneedles containing VEGF were capable of inducing tube formation to a small degree and cell proliferation to a reasonable degree. The standard cell proliferation assay provided evidence of cell proliferation in response to increasing levels of VEGF delivery through dissolved microneedle infusion. The integrated cell proliferation assay provided the most convincing evidence of successful microneedle delivery of bioactive protein drugs through a tissue phantom. In sum, the in-vitro studies suggest that VEGF maintains a degree of bioactivity after microneedle encapsulation; further in-vivo studies are required to determine whether the level of bioactivity of VEGF protein is sufficient to cause physiological, therapeutic effects in live biological systems.

3.8 In-Vivo Protein Bioactivity Assessment

In order to determine if the fabricated VEGF microneedles were functional in living biological systems, *in-vivo* experimentation was performed using standard laboratory mice under an institutional-approved protocol. In total, six microneedles were inserted into two mice, three per mouse as shown in Figure 8.

Representative images of the initial insertion of microneedles into the dorsal region of two mice is shown in Figure 26. Each of the three microneedles were spaced as far out as possible while conforming to the arrangement shown in Figure 8. Before insertion into the mouse skin, the microneedle arrays were observed to be well-formed and sharp. The post-insertion microneedle arrays were observed

to be partially dissolved, indicating that some quantity of polymer/VEGF solution was likely delivered through the skin.

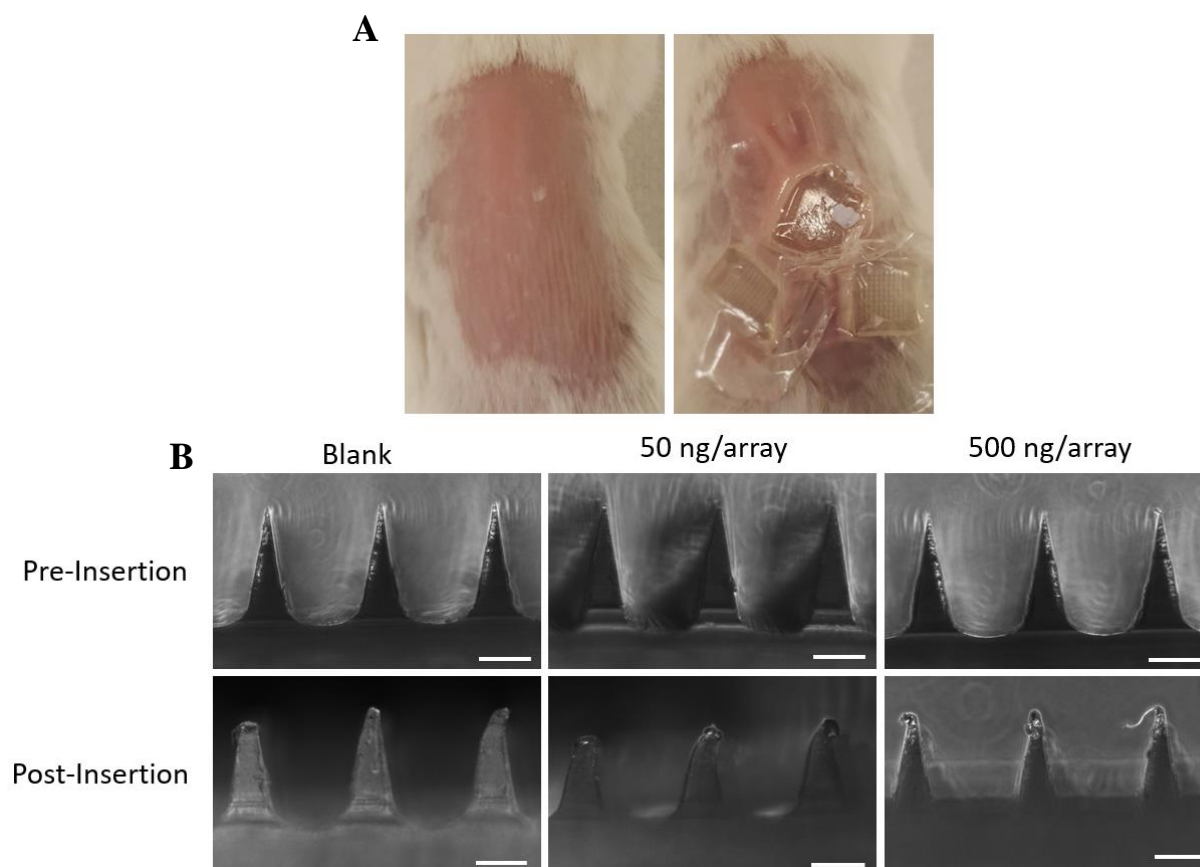


Figure 26. Insertion of Microneedles into Live Mice. A shows the shaved back of a female mouse with and without microneedle arrays inserted. B shows each of the three microneedle arrays before and after insertion into mouse skin. The scale bar shown is 200 μm .

Mice were visually evaluated daily for well-being and the presence of inflammation or erythema on the dorsal region. Figure 27 shows a representative image of the dorsal region of mice over seven days of observation. In general, there was no significant increase in inflammation following the insertion of VEGF encapsulating microneedles. The most perceptible change is between Day 5 and Day 6; however, the difference does not appear large enough to support the successful microneedle-mediated delivery of VEGF into the skin.

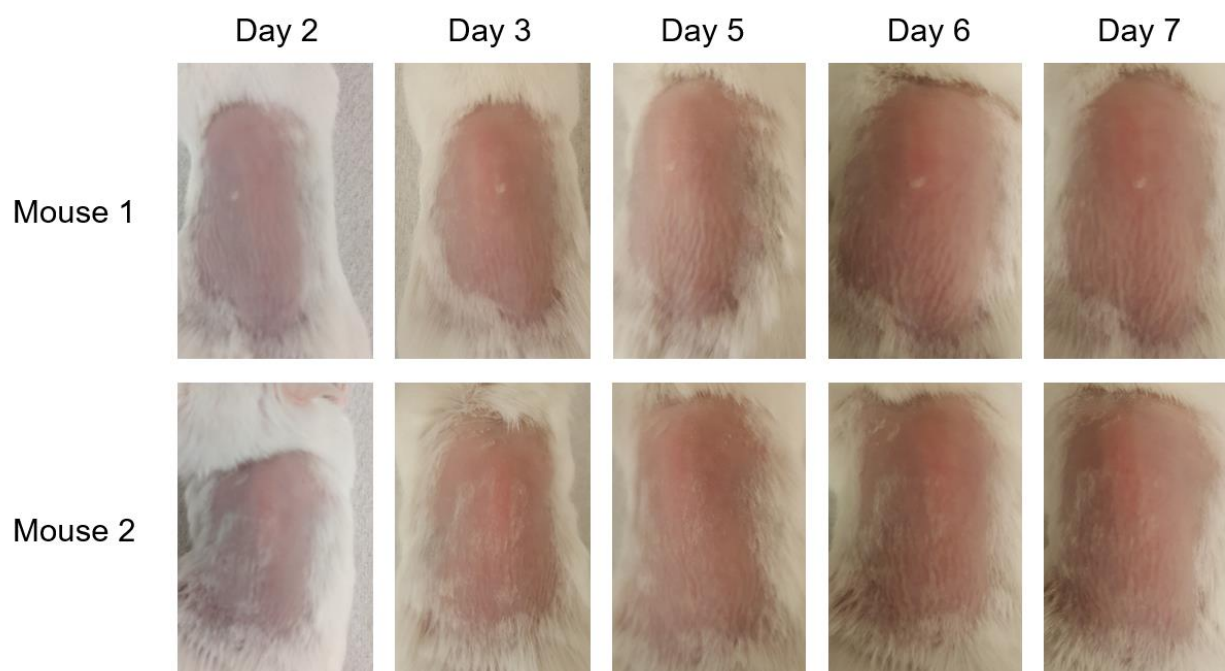


Figure 27. Inflammation on Dorsal Region of Mice. Day 1 was microneedle insertion. A perceptible but insignificant increase in inflammation is visible between Day 5 and Day 6. Day 3 was not captured due to technical error.

A significant limitation of this *in-vivo* animal study that may have prevented significant inflammation and erythema was limited microneedle penetration that resulted in inadequate dosing. As evident in Figure 26, microneedles were not fully dissolved upon insertion, resulting in reduced VEGF delivery compared to the *in-vitro* cell proliferation assay. One reason for diminished dissolution of the microneedles into the skin of the live mice was inadequate penetration of the outermost skin layer. It is thought that this is due to the lack of rigid bone structures at the specific insertion sites chosen on the dorsal region of mice. It is expected based on prior experimentation that single microneedle insertion on the center of the back of individual mice will result in greater insertion and ultimately improved drug delivery.

The integrated cell proliferation assay resulted in near complete dissolution of microneedles into the agarose tissue phantom, thus providing a sufficient source of VEGF to influence endothelial cell proliferation. Additionally, the microneedles were inserted completely into the tissue phantom due to the presence of a hard underlying surface.

Ongoing efforts are being made to execute successful *in-vivo* drug delivery and are incomplete as of the publishing of this thesis. It is thought that both increasing the dose of VEGF contained within the polymer microneedles as well as providing for a firmer surface to insert the needles will enable the successful *in-vivo* delivery of a therapeutic dose of VEGF.

Chapter 4

Conclusions and Future Research

4.1 Conclusions

This study encompassed the fabrication, characterization, and evaluation of polymeric microneedles capable of delivering the protein VEGF. The mechanical strength of PVA/PVP microneedles was found to be sufficiently strong to penetrate the skin and the model proteins BSA and VEGF were found to demonstrate adequate stability to enable successful encapsulation. The *in-vitro* tube formation and cell proliferation assays suggested reasonable bioactivity suitable for *in-vivo* experimentation to determine physiological effects in live animal systems. The *in-vivo* animal study results are indeterminate as of the publishing of this thesis, however ongoing efforts are being made to enact successful VEGF delivery in live mice.

4.2 Future Research

The results of this study have important considerations for the continual improvement of drug delivery devices in the treatment of patients. Future research may investigate sustained release methods with the goal of releasing protein drugs over a period of time as opposed to an immediate bolus release through the use of aptamer technology. Additionally, further research may incorporate different proteins of interest to target other pathologies. The biological effects of the specific polymer composition used in the microneedle matrix is also an important area of future research in order to mitigate adverse biological effects resulting from biomaterial interactions. Finally, microneedles may also be developed to deliver small quantities of proteins into systemic circulation, such as hormones or other chemical mediators in order to treat endocrine disorders.

BIBLIOGRAPHY

- [1] W. Sun *et al.*, “Polyvinylpyrrolidone microneedles enable delivery of intact proteins for diagnostic and therapeutic applications,” *Acta Biomater.*, vol. 9, no. 8, pp. 7767–7774, 2013.
- [2] M. R. Prausnitz, “Engineering Microneedle Patches for Vaccination and Drug Delivery to Skin,” *Annu. Rev. Chem. Biomol. Eng.*, vol. 8, no. 1, p. annurev-chembioeng-060816-101514, 2017.
- [3] B. J. Bruno, G. D. Miller, and C. S. Lim, “Basics and recent advances in peptide and protein drug delivery,” *Ther. Deliv.*, vol. 4, no. 11, pp. 1443–1467, 2014.
- [4] S. Li, N. Chen, E. R. Gaddes, X. Zhang, C. Dong, and Y. Wang, “A Drosera-bioinspired hydrogel for catching and killing cancer cells,” *Sci. Rep.*, vol. 5, pp. 1–12, 2015.
- [5] J. Coyne, B. Davis, D. Kauffman, and Y. Wang, “Polymer Microneedle Mediated Local Aptamer Delivery for Blocking the Function of Vascular Endothelial Growth Factor,” *ACS Biomater. Sci. Eng.*, 2017.
- [6] M. R. Battig, Y. Huang, N. Chen, and Y. Wang, “Aptamer-functionalized superporous hydrogels for sequestration and release of growth factors regulated via molecular recognition,” *Biomaterials*, vol. 35, no. 27, pp. 8040–8048, 2014.
- [7] B. Soontornworajit and Y. Wang, “Nucleic acid aptamers for clinical diagnosis: Cell detection and molecular imaging,” *Anal. Bioanal. Chem.*, vol. 399, no. 4, pp. 1591–1599, 2011.
- [8] N. G. Roupael *et al.*, “The safety, immunogenicity, and acceptability of inactivated influenza vaccine delivered by microneedle patch (TIV-MNP 2015): a randomised, partly blinded, placebo-controlled, phase 1 trial,” *Lancet*, vol. 6736, no. 17, pp. 1–10, 2017.
- [9] Y. C. Kim, J. H. Park, and M. R. Prausnitz, “Microneedles for drug and vaccine delivery,” *Adv. Drug Deliv. Rev.*, vol. 64, no. 14, pp. 1547–1568, 2012.
- [10] M. R. Prausnitz, J. A. Mikszta, M. Cormier, and A. K. Andrianov, “Microneedle-based vaccines,”

- Curr Top Microbiol Immunol.*, vol. 333, no. 1, pp. 369–393, 2009.
- [11] Y. C. Kim, B. Chiang, X. Wu, and M. R. Prausnitz, “Ocular delivery of macromolecules,” *J. Control. Release*, vol. 190, pp. 172–181, 2014.
- [12] J. R. Weiser and W. M. Saltzman, “Controlled release for local delivery of drugs: Barriers and models,” *J. Control. Release*, vol. 190, pp. 664–673, 2014.
- [13] Y. G. Anissimov, O. G. Jepps, Y. Dancik, and M. S. Roberts, “Mathematical and pharmacokinetic modelling of epidermal and dermal transport processes,” *Adv. Drug Deliv. Rev.*, vol. 65, no. 2, pp. 169–190, 2013.
- [14] L. Y. Chu, S. Choi, and M. R. Prausnitz, “Fabrication of Dissolving Polymer Microneedles for Controlled Drug Encapsulation and Delivery : Bubble and Pedestal Microneedle Designs,” vol. 99, no. 10, pp. 4228–4238, 2010.
- [15] K. Ita, “Transdermal delivery of drugs with microneedles—potential and challenges,” *Pharmaceutics*, vol. 7, no. 3, pp. 90–105, 2015.
- [16] R. G. Buckles, “Biomaterials for drug delivery systems.,” *J. Biomed. Mater. Res.*, vol. 17, pp. 109–128, 1983.
- [17] J. Arya, S. Henry, H. Kalluri, D. V. McAllister, W. P. Pewin, and M. R. Prausnitz, “Tolerability, usability and acceptability of dissolving microneedle patch administration in human subjects,” *Biomaterials*, vol. 128, pp. 1–7, 2017.
- [18] J. W. Lee, J. H. Park, and M. R. Prausnitz, “Dissolving microneedles for transdermal drug delivery,” *Biomaterials*, vol. 29, no. 13, pp. 2113–2124, 2008.
- [19] L. Y. Chu and M. R. Prausnitz, “Separable arrowhead microneedles,” *J. Control. Release*, vol. 149, no. 3, pp. 242–249, 2011.
- [20] J. E. Tengood, K. M. Kovach, P. E. Vescovi, A. Russel, and S. R. Little, “Sequential Delivery of Vascular Endothelial Growth Factor and Shingosine 1-Phosphate for Angiogenesis,” *Biomaterials*, vol. 31, no. 30, pp. 7805–7812, 2010.

- [21] T. Simón-Yarza, F. R. Formiga, E. Tamayo, B. Pelacho, F. Prosper, and M. J. Blanco-Prieto, “Vascular endothelial growth factor-delivery systems for cardiac repair: An overview,” *Theranostics*, vol. 2, no. 6, pp. 541–552, 2012.
- [22] J. S. Kochhar, S. Zou, S. Y. Chan, and L. Kang, “Protein encapsulation in polymeric microneedles by photolithography Protein encapsulation in polymeric microneedles by photolithography,” *Int. J. Nanomedicine*, vol. 7, no. June, pp. 3143–3154, 2012.
- [23] K. L. Decicco-skinner *et al.*, “Endothelial Cell Tube Formation Assay for the In Vitro Study of Angiogenesis,” vol. 10, no. September, pp. 1–8, 2014.
- [24] D. Zhang, D. B. Das, and C. D. Rielly, “Microneedle assisted micro-particle delivery by gene guns: Mathematical model formulation and experimental verification,” *Chem. Eng. Sci.*, vol. 125, no. 2, pp. 176–190, 2015.
- [25] I.-C. Lee, J.-S. He, M.-T. Tsai, and K.-C. Lin, “Fabrication of a novel partially dissolving polymer microneedle patch for transdermal drug delivery,” *J. Mater. Chem. B*, vol. 3, no. 2, pp. 276–285, 2015.
- [26] J. Park, M. G. Allen, and M. R. Prausnitz, “Biodegradable polymer microneedles : Fabrication , mechanics and transdermal drug delivery,” vol. 104, pp. 51–66, 2005.
- [27] V. K. Sharma and D. S. Kalonia, “Steady-state tryptophan fluorescence spectroscopy study to probe tertiary structure of proteins in solid powders,” *J. Pharm. Sci.*, vol. 92, no. 4, pp. 890–899, 2003.
- [28] National University of Singapore Department of Physics, “Fluorescence Spectroscopy : A tool for Protein folding / unfolding Study,” 2007.

ACADEMIC VITA

Academic Vita of David Kauffman

dmk5552@psu.edu

Education

Major: Biomedical Engineering

Honors: Biomedical Engineering

Thesis Title: Investigation of Polymer Microneedles in the Delivery of Protein Drugs

Thesis Supervisor: Dr. Yong Wang

Work Experience

January 2018 – May 2018

Chemistry Teaching Assistant

Penn State Department of Chemistry, University Park, PA

August 2017 – May 2018

Guided Study Group Leader

Penn State Learning, University Park, PA

June 2011 – July 2016

Aquatics Supervisor, Swim Team Coach, Lifeguard

Lake Naomi Club, Pocono Pines, PA

Grants: Academic Excellence Scholarship, Provost's Scholarship, Goebert College of Engineering Scholarship, Penn State Erickson Discovery Grant, Whitman Fund Grant.

Awards: President's Freshman Award, President Sparks Award.

Publications: Coyne, J. Davis, B. Kauffman, D. Zhao, N. Wang, Y. Polymer Microneedle Mediated Local Aptamer Delivery for Blocking the Function of Vascular Endothelial Growth Factor. ACS Biomater. Sci. Eng. 2017. DOI: 10.1021/acsbomaterials.7b00718

Presentations: Kauffman, D. Davis, B. Coyne, J. Wang, Y. Sustained Release of Protein Drugs from Polymeric Microneedles for Immunotherapy. 2017 Biomedical Engineering Society Annual Meeting, Phoenix, AZ.